*Inorg. Chem.* **1998,** *37,* 6615−6629

# Synthesis and Characterization of a Family of Systematically Varied Tris(2-pyridyl)methoxymethane Ligands: Copper(I) and Copper(II) Complexes

**Robert T. Jonas and T. D. P. Stack***

Department of Chemistry, Stanford University Stanford, California 94305-5080

*Received October 23, 1997*

An efficient modular protocol for synthesizing a series of facial-capping tris-pyridyl ligands, based on the tris-(2-pyridyl)methoxymethane backbone, has been developed which allows for systematic variations of the steric demands at the periphery of the ligand. The coordination chemistry of one such family of ligands that positions 0→3 methoxy groups at the periphery with Cu(I) and Cu(II) is presented. The ligands are tris(2-pyridyl)-methoxymethane ($\mathbf{L^0}$), bis(2-pyridyl)(2-(6-methoxy)pyridyl)methoxymethane ($\mathbf{L^1}$), bis(2-(6-methoxy)pyridyl)(2-pyridyl)methoxymethane ($\mathbf{L^2}$), and tris(2-(6-methoxy)pyridyl)methoxymethane ($\mathbf{L^3}$). The ligand exchange behavior and, to a lesser extent, the structures of the these complexes vary dramatically given the small perturbation of introducing methoxy substituents. Two distinct coordination modes are observed for the Cu(I) complexes, both in solution and the solid state. One is a pseudo-tetrahedral coordination comprised of the facial-capping, tris-pyridyl ligand and a monodentate ligand such as $CH_3CN$, CO, or $PPh_3$. The other structural type is also a pseudo-tetrahedral Cu(I) monomer formed by two tris-pyridyl ligands coordinated in a bidentate manner with preferable binding by the nonmethoxy pyridyl subunits. With the exception of the most sterically hindered ligand, $\mathbf{L^3}$, which only displays monoligation to Cu(I), all ligands form both types of Cu(I) complexes, and the formation is controlled by stoichiometry. Both competitive ligand binding experiments and ligand substitution with CO(g) show that the $[(\mathbf{L^0})_2\mathrm{Cu}]^+$ and $[(\mathbf{L^1})_2\mathrm{Cu}]^+$ complexes have nearly equivalent stability in aprotic solvent, and greater stability than the $[(\mathbf{L^2})_2\mathrm{Cu}]^+$ complex due to inclusion of bulky methoxypyridines into the Cu(I) coordination sphere. The Cu(II) complexes of the ligand series generate “bis-tris”, $[(\mathbf{L^{0\rightarrow3}})_2\mathrm{Cu}]^{2+}$, complexes, with the Cu(II) ligated in a tetragonally distorted octahedral coordination environment. The degree of bulk at the ligand periphery dictates the Cu(II)-ligand bond lengths both in solution and the solid state. In these complexes, the bulky pyridyl ring prefers to bind in the axial position. For the most sterically encumbered ligand, $\mathbf{L^3}$, the bisligated Cu(II) complex is moisture sensitive, reacting to give a monoligated, tris-aqua species, $[\mathbf{L^3}\mathrm{Cu}(H_2O)_3]^{2+}$.

## Introduction

Metalloenzymes have evolved very specific structural environments to control the reactivity at the metal center. Seemingly subtle structural variations in the near vicinity of the coordination site can dramatically change the enzyme reactivity. Systematic studies which correlate the structural parameters to the enzyme function are limited, though the recent wealth of structural information from appropriately mutated proteins along with their reactivity is much more assessable with the advances in protein crystallography.[1] Synthetic model complexes are well suited for systematic studies to understand the interplay of structural perturbations on chemical reactivity of a particular metal. The structure−function trends discovered are often applicable to the native system. An important component of many successful model systems is the inclusion of sterically demanding groups near the metal coordination site of the ligand. These groups not only provide a protective cavity for the metal, precluding undesired bimolecular reactions in solution, but also can indirectly distort the metal coordination leading to different reactivity properties. Systematic synthetic variations of these protective groups assists in the correlation of reactivity properties with structure at a molecular level of detail generally not available in proteins.[2] With these considerations, a ligand with an efficient and highly versatile synthesis is advantageous.[3]

Numerous biological enzymes are known to facilitate the reaction of dioxygen by utilizing multinuclear Cu(I) metal sites.[4−8] A common structural characteristic of these copper sites is the tris-imidazole ligation of three histidine residues in both the oxidized and reduced form.[9−11] Copper complexes of symmetrical facial-capping, tridentate nitrogen ligands, such as tris(pyrazoyl)hydroborate,[5,12,13] 1,4,7-triazacyclononane,[14,15]

---

* Corresponding author. Telefax: (650) 725-0259. E-mail: stack@leland.stanford.edu.

(1) Holm, R. H.; Kennepohl, P.; Solomon, E. I. *Chem. Rev.* **1996**, *96*, 2239−2314.

(2) Ibers, J. A.; Holm, R. H. *Science* **1980**, *209*, 223−235.

(3) Sorrell, T. N. *Tetrahedron* **1989**, *45*, 3−68.

(4) *Bioinorganic Chemistry of Copper*; Karlin, K. D., Tyeklár, Z., Eds.; Chapman & Hall: New York, 1993.

(5) Kitajima, N.; Moro-oka, Y. *Chem. Rev.* **1994**, *94*, 737−757.

(6) Karlin, K. D.; Fox, S. In *Active Oxygen in Biochemistry*; Valentine, J. S., Foote, C. S., Greenberg, A., Liebman, J. F., Eds.; Chapman & Hall: Glasgow, 1995; Vol. 3, p 188−231.

(7) Klinman, J. P. *Chem. Rev.* **1996**, *96*, 2541−2562.

(8) Solomon, E. I.; Sundaram, U. M.; Machonkin, T. E. *Chem. Rev.* **1996**, *96*, 2563−2606.

(9) Godden, J. W.; Turley, S.; Teller, D. C.; Adman, E. T.; Liu, M. Y.; Payne, W. J.; LeGall, J. *Science* **1991**, *253*, 438−442.

(10) Messerschmidt, A.; Luecke, H.; Huber, R. *J. Mol. Biol.* **1993**, *230*, 997−1014.

(11) Magnus, K. A.; Ton-That, H.; Carpenter, J. E. *Chem. Rev.* **1994**, *94*, 727−735.

(12) Thompson, J. S.; Whitney, J. F. *Inorg. Chem.* **1984**, *23*, 2813−2819.

(13) Kitajima, N.; Fujisawa, K.; Fujimoto, C.; Moro-oka, Y.; Hashimoto, S.; Kitagawa, T.; Toriumi, K.; Tatsumi, K.; Nakamura, A. *J. Am. Chem. Soc.* **1992**, *114*, 1277−1291.

(14) Wieghardt, K.; Chaudhuri, P. *Prog. Inorg. Chem.* **1988**, *35*, 329−436.

10.1021/ic9713487 CCC: $15.00 © 1998 American Chemical Society
Published on Web 12/28/1998

**Chart 1**

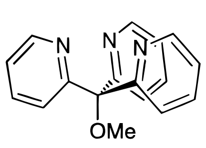

**L⁰**

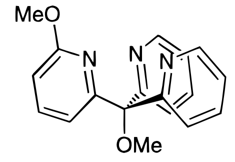

**L¹**

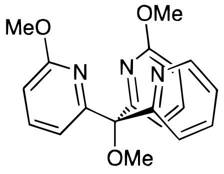

**L²**

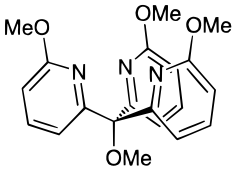

**L³**

tris(imidazole)methoxymethane,[16,17] and tris(imidazole)phosphine,[18−20] constitute an important class of biomimetic copper model systems which have aided in elucidating the structural, electronic, and chemical properties of the biological copper oxygenases in recent years.[5,8,15,21]

Tris(2-pyridyl)carbinol (TPC) is a symmetric, facial-capping trinitrogen ligand, but its metal chemistry has not been extensively explored since its original synthesis almost fifty years ago.[16,22−26] The stepwise synthesis of TPC allows for myriad substitutions to this ligand template, which is not always the case for other parent ligand templates. Other facial-capping, trinitrogen ligands, while readily prepared, are often difficult to modify or purify. By exploiting the synthetic versatility in the preparation of TPC, we have generated a family of ligands that incorporates 0→3 methoxy groups at the periphery of the coordination cavity (Chart 1). These methoxy substituents are readily introduced into the ligands to give moderate steric bulk without sacrificing the high yield and ease of purification of the parent TPC ligand. Successful chelation of both Cu(I) and Cu(II) is achieved with all four ligands. The degree of substitution at the ligand periphery directly effects the preferred binding mode of the ligand and ligand substitution reactions of these copper complexes. A systematic study of the simple Cu(I) and Cu(II) complexes of these ligands is necessary before these ligands are used as modular building units in the construction of poly-nucleating ligands.

## Experimental Section[27]

**Syntheses.** All starting materials were purchased from Aldrich and used without further purification except for the following: $[Cu^I(CH_3CN)_4](OTf)$[28] and $Cu^{II}(OTf)_2$[29] were synthesized by modifications of the literature methods. Sodium hydride (60% oil dispersion) was washed with hexanes and dried in a vacuum. All solvents and gases were of analytical grade and were purified by literature methods.[30] $CH_2Cl_2$ was distilled from $CaH_2$ under $N_2$ and stored over 4 Å molecular sieves. $CH_3CN$ was distilled from $CaH_2$ under $N_2$. Anhydrous diethyl ether (ether) was stored over 4 Å molecular sieves. THF was distilled from NaK under $N_2$. All solutions were degassed prior to use. All copper complexes were synthesized and handled under a $N_2$ inert atmosphere using a MBraun Labmaster 130 glovebox or standard Schlenk-line techniques. All chromatography was performed using silica gel #60 from EM Science using standard techniques for flash chromatography.[31]

**Instrumentation.** Infrared spectra were recorded in either a NaCl solution cell or a solid KBr matrix on a Perkin-Elmer 1600 series FT-IR spectrophotometer. $^1H$ and $^{13}C$ NMR spectra were recorded on either a Varian Gemini-200 (200 MHz) or a Varian Gemini-400 (400 MHz) NMR spectrometer at room temperature (RT), and chemical shifts are reported in ppm downfield from an internal TMS reference. Electronic spectra at RT were measured on a Hewlett-Packard 8452A UV/vis diode array spectrophotometer. EPR spectra were recorded on a Bruker ER 220D-SRC instrument as frozen solutions at 77 K in quartz tubes. Electrochemical measurements were recorded in either $CH_3CN$ or $CH_2Cl_2$ solutions by using standard PAR instrumentation, a platinum working electrode, a platinum wire auxiliary electrode, 0.1 M $(n\text{-}Bu_4N)(ClO_4)$ supporting electrolyte, and a Ag/AgCl reference electrode. Unless noted otherwise, cyclic voltammetry data were recorded at 100 mV/s in the drybox at RT, with all potentials measured against $E_{1/2}$ (ferrocenium/ferrocene, $Fc/Fc^+$) but reported relative to the SCE ($E_{1/2}$ versus $Fc/Fc^+ = +0.450$ V in $CH_3CN$). Representative elemental analyses of specific complex types were conducted by Desert Analytics (Tucson, AZ). Mass spectra were performed by the Mass Spectroscopy Facility at the University of California at San Francisco.

**Ligand Syntheses. Bis(2-(6-methoxy)pyridyl)ketone.** To 2-bromo-6-methoxypyridine[32] (8.81 g, 0.0468 mol) in THF (100 mL) at −78 °C, n-BuLi (2.5 M in hexanes, 19.0 mL, 0.0475 mol) is added dropwise to maintain the temperature of the solution below −60 °C. Ethylchloroformate (2.30 mL, 2.61 g, 0.0240 mol) in THF cooled to −78 °C is slowly added to the yellow solution to give a deep green solution. After 1 h, MeOH (50 mL) is added to the reaction mixture at −78 °C and warmed to RT. Water (50 mL) and 10% HCl (50 mL) are added, the organic solvents are removed under vacuum, and the product is extracted with $CH_2Cl_2$. Chromatography (10% EA/H) yields an oily residue that is crystallized from 10% ether/hexanes to give a slightly yellow solid (5.12 g, 90% yield). $^1H$ NMR (200 MHz, $CDCl_3$): 3.91 (6 H, s, py-OMe), 6.93 (2 H, d of d, $J_1 = 6.6$ Hz, $J_2 = 2.6$ Hz, 5-Hpy), 7.70 (2 H, s, 4-Hpy), 7.72 (2 H, d, $J = 4.2$ Hz, 3-Hpy). MS ($FAB^+$, $MH^+$): *m*/*e* 245.1 (EM = 244.1).

**Ligand Series.** The stepwise syntheses of the ligands from their respective ketones and lithiopyridines are very similar (Schemes 1 and 2). A representative example is given for the synthesis of $\mathbf{L^0}$ from bis(2-pyridyl)ketone and 2-lithiopyridine.

**Tris(2-pyridyl)methoxymethane ($\mathbf{L^0}$) and Tris(2-pyridyl)methoxy-$\boldsymbol{d_3}$-methane ($\mathbf{L^0\text{-}d_3}$).** Prepared by a modification of the literature procedure.[22] A THF solution of 2-bromopyridine (2.50 mL, 4.14 g, 0.0262 mol) is cooled to −78 °C and n-BuLi (2.5 M, 11.0 mL, 0.028 mol) is added dropwise to maintain the temperature below −60 °C. A THF solution of bis(2-pyridyl)ketone (4.52 g, 0.0245 mol) at −78 °C

---

(15) Tolman, W. B. *Acc. Chem. Res.* **1997**, *30*, 227−237 and references therein.
(16) Brown, R. S.; Huguet, J. *Can. J. Chem.* **1980**, *58*, 889−901.
(17) Sorrell, T. S.; Borovik, A. S. *J. Am. Chem. Soc.* **1987**, *109*, 4255−4260.
(18) Allen, W. E.; Sorrell, T. N. *Inorg. Chem.* **1997**, *36*, 1732−1734.
(19) Sorrell, T. N.; Allen, W. E.; White, P. S. *Inorg. Chem.* **1995**, *34*, 952−960.
(20) Lynch, W. E.; Kurtz, D. M.; Wang, S. K.; Scott, R. A. *J. Am. Chem. Soc.* **1994**, *116*, 11030−11038.
(21) Karlin, K. D.; Kaderli, S.; Zuberbühler, A. D. *Acc. Chem. Res.* **1997**, *30*, 139−147.
(22) Wibaut, J. P.; de Jonge, A. P.; Van der Voort, H. G. P.; Otto, H. L. *Recl. Trav. Chim. Pays-Bas* **1951**, *70*, 1054−1066.
(23) Boggess, R. K.; Boberg, S. *J. Inorg. Nucl. Chem.* **1980**, *42*, 21−26.
(24) Canty, A. J.; Chaichit, N.; Gatehouse, B. M.; George, E. E. *Inorg. Chem.* **1981**, *20*, 4293−4300.
(25) Canty, A. J.; Minchin, N. J.; Healy, P. C.; White, A. H. *J. Chem. Soc., Dalton Trans.* **1982**, 1795−1802.
(26) Keene, F. R.; Szalda, D. J.; Wilson, T. A. *Inorg. Chem.* **1987**, *26*, 2211−2216.
(27) Abbreviations: THF, tetrahydrofuran; DMF, *N*,*N*-dimethylformamide; $CH_2Cl_2$, dichloromethane; $CH_3CN$, acetonitrile; MeOH, methanol; EPR, electron paramagnetic resonance; FT, Fourier transform; FAB, fast atom bombardment; s, singlet; d, doublet; t, triplet; q, quintet; m, multiplet; br, broad; EA/H, ethyl acetate/hexanes.
(28) Haynes, J. S.; Sams, J. R.; Thompson, R. C. *Can. J. Chem.* **1981**, *59*, 669−678.
(29) Jenkins, C. L.; Kochi, J. K. *J. Am. Chem. Soc.* **1972**, *94*, 843−856.
(30) Perrin, D. D.; Armarego, W. L. F. *Purification of Laboratory Chemicals*; Pergamon Press: New York, 1988.
(31) Still, W. C.; Kahn, M.; Mitra, A. *J. Org. Chem.* **1978**, *43*, 2923−2925.
(32) Testaferri, L.; Tiecco, M.; Tingoli, M.; Bartoli, D.; Massoli, A. *Tetrahedron* **1985**, *41*, 1373−1384.

**Scheme 1**

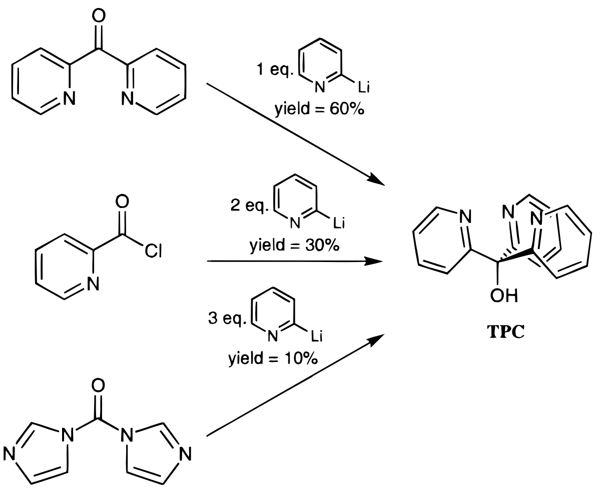

**Scheme 2**

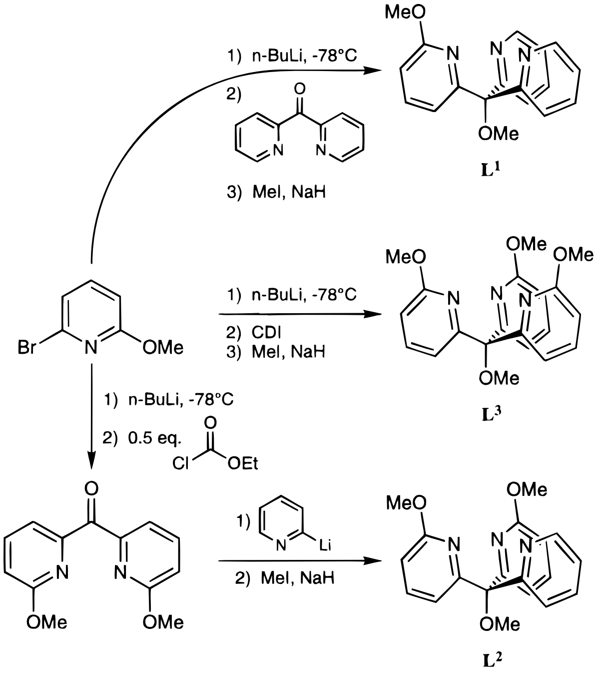

is slowly added to initially give a deep red solution that eventually becomes deep blue and finally a dull purple after 1 h. The reaction is quenched with MeOH (25 mL), and warmed to RT to give a light orange solution. After the addition of water (50 mL) and 10% HCl (50 mL), the organic solvents are removed. The tris(2-pyridyl)carbinol product is extracted with $CH_2Cl_2$ and recrystallized from acetone (4.1 g, 60% yield). NaH (1.63 g, 0.0611 mol) is added to a DMF solution of the tris-pyridylcarbinol at RT. Iodomethane (0.80 mL, 1.8 g, 0.013 mol) is added dropwise to give a cloudy beige solution. The solution is stirred for 1.5 h and quenched with a 1:1 mixture of acetone and 2-propanol. After water addition, the organic solvents are removed under vacuum. The product is extracted with $CH_2Cl_2$ and recrystallized from acetone to give a crystalline white solid (3.2 g, 50% total yield). $^1$H NMR (200 MHz, $CDCl_3$): 3.29 (3 H, s, C−OMe), 7.19 (3 H, t of d, $J_1 = 5.0$ Hz, $J_2 = 3.2$ Hz, 5-Hpy), 7.70 (3 H, t, $J = 1.6$ Hz, 4-Hpy), 7.73 (3 H, d, $J = 1.4$ Hz, 3-Hpy), 8.62 (3 H, d, $J = 4.8$ Hz, 6-Hpy). MS (FAB$^+$, MH$^+$): *m/e* 278.2 (EM = 277.1). $\mathbf{L^0}$-$d_3$ is synthesized in an analogous manner except that iodomethane-$d_3$ is used. A $^1$H NMR spectrum is identical to $\mathbf{L^0}$ excluding the bridgehead methoxy resonance; integration indicates >99% deuterium incorporation.

**Bis(2-pyridyl)(2-(6-methoxy)pyridyl)methoxymethane ($\mathbf{L^1}$) and Bis(2-pyridyl)(2-(6-methoxy)pyridyl)methoxy-$d_3$-methane ($\mathbf{L^1}$-$d_3$).** The impure tris-pyridylcarbinol formed from the reaction of 2-lithio-6-methoxypyridine and bis(2-pyridyl)ketone is purified by chromatography (20% EA/H) prior to methylation. The methylated product is isolated as a yellow oil by chromatography (50% EA/H) and recrystallized from ether to give a crystalline white solid (80% yield). $^1$H NMR (200 MHz, $CDCl_3$): 3.32 (3 H, s, C−OMe), 3.67 (3 H, s, py-OMe), 6.61 (1 H, d, $J = 8.2$ Hz, 5-Hpy(OMe)), 7.15 (2 H, t of d, $J_1 = 5.0$ Hz, $J_2 = 3.2$ Hz, 5-Hpy), 7.23 (1 H, d, $J = 7.4$ Hz, 3-Hpy(OMe)), 7.57 (1 H, t, $J = 9.8$ Hz, 4-Hpy(OMe)), 7.65 (2 H, t, $J = 1.6$ Hz, 4-Hpy), 7.68 (2 H, d, $J = 1.6$ Hz, 3-Hpy), 8.59 (2 H, d, $J = 4.0$ Hz, 6-Hpy). MS (FAB$^+$, MH$^+$): *m/e* 308.2 (EM = 307.1). $\mathbf{L^1}$-$d_3$ is synthesized in an analogous manner except that iodomethane-$d_3$ is used. A $^1$H NMR spectrum is identical to $\mathbf{L^1}$ excluding the bridgehead methoxy resonance; integration indicates >99% deuterium incorporation.

**Bis(2-(6-methoxy)pyridyl)(2-pyridyl)methoxymethane ($\mathbf{L^2}$) and Bis(2-(6-methoxy)pyridyl)(2-pyridyl)methoxy-$d_3$-methane ($\mathbf{L^2}$-$d_3$).** The impure tris-pyridylcarbinol formed from the reaction of 2-lithiopyridine and bis(2-(6-methoxy)pyridyl)ketone is purified by chromatography (10% EA/H) prior to methylation. The methylated product is isolated as a yellow oil by chromatography (25% EA/H) that solidifies to give a crystalline beige solid (75% yield). $^1$H NMR (200 MHz, $CDCl_3$): 3.33 (3 H, s, C−OMe), 3.67 (6 H, s, py-OMe), 6.58 (2 H, d, $J = 8.0$ Hz, 5-Hpy(OMe)), 7.12 (1 H, t of d, $J_1 = 5.0$ Hz, $J_2 = 2.2$ Hz, 5-Hpy), 7.22 (2 H, d, $J = 7.2$ Hz, 3-Hpy(OMe)), 7.54 (2 H, t, $J = 9.2$ Hz, 4-Hpy(OMe)), 7.64 (1 H, t, $J = 1.6$ Hz, 4-Hpy), 7.70 (1 H, d, $J = 1.6$ Hz, 3-Hpy), 8.58 (1 H, d, $J = 4.0$ Hz, 6-Hpy). MS (FAB$^+$, MH$^+$): *m/e* 338.2 (EM = 337.1). $\mathbf{L^2}$-$d_3$ is synthesized in an analogous manner except that iodomethane-$d_3$ is used. A $^1$H NMR spectrum is identical to $\mathbf{L^2}$ excluding the bridgehead methoxy resonance; integration indicates >99% deuterium incorporation.

**Tris(2-(6-methoxy)pyridyl)methoxymethane ($\mathbf{L^3}$).** The ligand can be synthesized by two methods. (a) The impure tris-pyridylcarbinol formed from the reaction of 2-lithio-6-methoxypyridine[32] and bis(2-(6-methoxy)pyridyl)ketone is purified by chromatography (10% EA/H) prior to methylation. The methylated product is isolated as a yellow oil by chromatography (20% EA/H) (85% yield). (b) The direct synthesis of the tris-pyridylcarbinol using 3 equiv of 2-lithio-6-methoxypyridine and 1 equiv of carbonyldiimidazole (CDI) results in reasonable yields. To a THF solution of 2-bromo-6-methoxypyridine (6.60 g, 0.0351 mol) at −78 °C, n-BuLi (2.5 M, 14.4 mL, 0.0360 mol) is added dropwise to maintain the solution below −60 °C. A THF solution of CDI (1.654 g, 0.0102 mol) at −78 °C is added slowly to give a dark purple/brown solution. After 2 h, the reaction is quenched with MeOH (25 mL), and warmed to RT. After the addition of water (50 mL) and 10% HCl (50 mL), the organic solvents are removed under vacuum. The product is extracted with $CH_2Cl_2$ and purified by chromatography (15% EA/H) to give the tris-pyridylcarbinol. The methylated product is isolated as a yellow oil by chromatography (20% EA/H) (80% yield). $^1$H NMR (200 MHz, $CDCl_3$): 3.40 (3 H, s, C−OMe), 3.72 (9 H, s, py-OMe), 6.58 (3 H, d, $J = 8.2$ Hz, 5-Hpy-(OMe)), 7.19 (3 H, d, $J = 7.4$ Hz, 3-Hpy(OMe)), 7.52 (3 H, t, $J = 8.0$ Hz, 4-Hpy(OMe)). MS (FAB$^+$, MH$^+$): *m/e* 368.2 (EM = 367.2).

**Syntheses of Metal Complexes [$\mathbf{L^{0-3}Cu^I(CH_3CN)}$](OTf).** Each of the four Cu(I) complexes are synthesized in acetone with equimolar amounts of ligand, **L** (**L** = $\mathbf{L^{0-3}}$), and [Cu$^I$(CH$_3$CN)$_4$](OTf).

**[$\mathbf{L^0Cu(CH_3CN)}$](OTf).** Anaerobic solutions of this complex degrade over the course of a week by disproportionation to give the bis-ligated Cu(II) complex, [($\mathbf{L^0}$)$_2$Cu](OTf)$_2$. The product could be isolated in moderate yields by quick evaporation of the solution. X-ray-quality yellow/green crystals of the complex are obtained from an acetone solution of the complex layered with hexanes. $^1$H NMR (400 MHz, acetone-$d_6$): 2.34 (3 H, s, $CH_3CN$), 3.78 (3 H, br s, C−OMe), 7.51 (3 H, br t, $J = 3.0$ Hz, 5-Hpy), 8.06 (3 H, br t, $J = 2.6$ Hz, 4-Hpy), 8.07 (3 H, d, $J = 5.0$ Hz, 3-Hpy), 8.71 (3 H, br d, 6-Hpy).

**[$\mathbf{L^1Cu(CH_3CN)}$](OTf).** The product is isolated as an oil, which is indefinitely stable under anaerobic conditions. $^1$H NMR (400 MHz, acetone-$d_6$): 2.35 (3 H, s, $CH_3CN$), 3.44 (3 H, s, C−OMe), 3.69 (3 H, s, py-OMe), 6.94 (1 H, d, $J = 8.2$ Hz, 5-Hpy(OMe)), 6.98 (1 H, d, $J = 7.3$ Hz, 3-Hpy(OMe)), 7.53 (2 H, t, $J = 5.4$ Hz, 5-Hpy), 7.85 (1 H, t, $J = 8.2$ Hz, 4-Hpy(OMe)), 8.10 (2 H, d, $J = 7.2$ Hz, 3-Hpy), 8.13 (2 H, t, $J = 3.0$ Hz, 4-Hpy), 8.66 (2 H, br s, 6-Hpy).

**[L$^2$Cu(CH$_3$CN)](OTf).** The solvent is reduced under vacuum, then hexanes are added to the solution to give the product as a yellow/white precipitate in nearly quantitative yield. $^1$H NMR (200 MHz, acetone-$d_6$): 2.36 (3 H, s, $CH_3CN$), 3.36 (3 H, s, C−OMe), 3.81 (6 H, s, py-OMe), 7.02 (2 H, d, $J = 8.4$ Hz, 5-Hpy(OMe)), 7.33 (2 H, d, $J = 7.5$ Hz, 3-Hpy(OMe)), 7.54 (1 H, t, $J = 5.2$ Hz, 5-Hpy), 7.97 (2 H, t, $J = 7.6$ Hz, 4-Hpy(OMe)), 8.10 (1 H, d, $J = 5.2$ Hz, 3-Hpy), 8.12 (1 H, t, $J = 3.0$ Hz, 4-Hpy), 8.65 (1 H, br d, $J = 5.0$ Hz, 6-Hpy).

**[L$^3$Cu(CH$_3$CN)](OTf).** After removal of the solvent, the product is recrystallized from acetone/ether. Exposure to air results in the formation of a Cu(II) complex with spectral characterization similar to the tris-aqua species, [**L$^3$**Cu(H$_2$O)$_3$](OTf)$_2$. Crystals suitable for X-ray-quality light yellow/green cubic crystals of the complex are obtained from vapor diffusion of ether into an acetone solution. $^1$H NMR (400 MHz, acetone-$d_6$): 2.34 (3 H, s, $CH_3CN$), 3.31 (3 H, s, C−OMe), 3.87 (9 H, s, py-OMe), 7.07 (3 H, d, $J = 8.0$ Hz, 5-Hpy(OMe)), 7.46 (3 H, d, $J = 7.4$ Hz, 3-Hpy(OMe)), 8.03 (3 H, t, $J = 8.0$ Hz, 4-Hpy(OMe)). Elem. anal. Calcd for $C_{23}H_{24}N_4O_7F_3SCu$: C, 44.48; H, 3.90; N, 9.02. Found: C, 44.93; H, 3.76; N, 9.06.

**Syntheses of Metal Complexes [L$^{0\rightarrow3}$Cu$^I$(X)](OTf); X = CO, PPh$_3$.** Displacement of the CH$_3$CN adduct in [**L**Cu(CH$_3$CN)]$^+$ (**L** = **L$^{0\rightarrow3}$**) with 1 atm of CO(g) or 1 equiv of PPh$_3$ gives the corresponding substituted complexes. Both the CO and PPh$_3$ adducts are isolated as nearly colorless microcrystalline powders from acetone/hexanes. Displacement of CO with 1 equiv of PPh$_3$ also gives the PPh$_3$ adduct indirectly.

**[L$^0$Cu(CO)](OTf).** $^1$H NMR (400 MHz, acetone-$d_6$): 4.02 (3 H, br s, C−OMe), 7.56 (3 H, br t, $J = 4.0$ Hz, 5-Hpy), 8.15 (3 H, br d, 6-Hpy), 8.20 (3 H, br t, $J = 2.6$ Hz, 4-Hpy), 9.01 (3 H, d, $J = 5.0$ Hz, 3-Hpy). FT-IR (CH$_2$Cl$_2$): $\nu$(CO) 2102 cm$^{-1}$.

**[L$^0$Cu(PPh$_3$)](OTf).** $^1$H NMR (400 MHz, acetone-$d_6$): 4.00 (3 H, br s, C−OMe), 7.25−7.65 (15 H, m, Ph), 7.41 (3 H, t, $J = 5.8$ Hz, 5-Hpy), 8.12 (3 H, t, $J = 6.4$ Hz, 4-Hpy), 8.23 (3 H, d, $J = 8.0$ Hz, 3-Hpy), 8.31 (3 H, br d, 6-Hpy).

**[L$^1$Cu(CO)](OTf).** $^1$H NMR (400 MHz, acetone-$d_6$): 3.97 (3 H, s, C−OMe), 4.09 (3 H, s, py-OMe), 7.19 (1 H, d, $J = 8.3$ Hz, 5-Hpy(OMe)), 7.62 (2 H, t, $J = 5.0$ Hz, 5-Hpy), 7.76 (1 H, d, $J = 7.9$ Hz, 3-Hpy(OMe)), 8.16 (1 H, t, $J = 7.8$ Hz, 4-Hpy(OMe)), 8.19 (2 H, t, $J = 1.6$ Hz, 4-Hpy), 8.20 (2 H, d, $J = 4.0$ Hz, 3-Hpy), 8.99 (2 H, br d, $J = 4.8$ Hz, 6-Hpy). FT-IR (CH$_2$Cl$_2$): $\nu$(CO) 2100 cm$^{-1}$.

**[L$^1$Cu(PPh$_3$)](OTf).** Colorless platelike crystals suitable for X-ray analysis are grown from a solution of the complex in acetone layered with hexanes. $^1$H NMR (400 MHz, acetone-$d_6$): 3.21 (3 H, s, py-OMe), 3.90 (3 H, s, C−OMe), 6.92 (1 H, d, $J = 8.5$ Hz, 5-Hpy(OMe)), 7.25−7.65 (15 H, m, Ph), 7.40 (2 H, br t, $J = 3.0$ Hz, 5-Hpy), 7.71 (1 H, d, $J = 7.6$ Hz, 3-Hpy(OMe)), 8.01 (1 H, t, $J = 7.9$ Hz, 4-Hpy(OMe)), 8.11 (2 H, t, $J = 7.7$ Hz, 4-Hpy), 8.20 (2 H, d, $J = 8.2$ Hz, 3-Hpy), 8.27 (2 H, d, $J = 5.0$ Hz, 6-Hpy).

**[L$^2$Cu(CO)](OTf).** $^1$H NMR (200 MHz, acetone-$d_6$): 3.95 (3 H, s, C−OMe), 4.11 (6 H, s, py-OMe), 7.18 (2 H, d, $J = 8.4$ Hz, 5-Hpy(OMe)), 7.60 (1 H, d of d, $J = 4.0$ Hz, 5-Hpy), 7.76 (2 H, d, $J = 8.0$ Hz, 3-Hpy(OMe)), 8.15 (2 H, t, $J = 7.8$ Hz, 4-Hpy(OMe)), 8.15 (1 H, d, $J = 4.0$ Hz, 3-Hpy), 8.17 (1 H, t, $J = 3.2$ Hz, 4-Hpy), 8.97 (1 H, d, $J = 5.0$ Hz, 6-Hpy). FT-IR (CH$_2$Cl$_2$): $\nu$(CO) 2096 cm$^{-1}$.

**[L$^2$Cu(PPh$_3$)](OTf).** $^1$H NMR (400 MHz, acetone-$d_6$): 3.27 (6 H, s, py-OMe), 3.73 (3 H, s, C−OMe), 6.91 (2 H, d, $J = 8.2$ Hz, 5-Hpy(OMe)), 7.25−7.65 (15 H, m, Ph), 7.40 (1 H, d of d, $J = 2.0$ Hz, 5-Hpy), 7.67 (2 H, d, $J = 7.3$ Hz, 3-Hpy(OMe)), 7.96 (2 H, t, $J = 8.2$ Hz, 4-Hpy(OMe)) 8.11 (1 H, t, $J = 7.7$ Hz, 4-Hpy), 8.19 (1 H, d, $J = 8.2$ Hz, 3-Hpy), 8.25 (1 H, d, $J = 5.0$ Hz, 6-Hpy).

**[L$^3$Cu(CO)](OTf).** $^1$H NMR (200 MHz, acetone-$d_6$): 3.93 (3 H, s, C−OMe), 4.11 (3 H, s, py-OMe), 7.18 (3 H, d, $J = 8.4$ Hz, 5-Hpy(OMe)), 7.74 (3 H, d, $J = 7.7$ Hz, 3-Hpy(OMe)), 8.14 (3 H, t, $J = 8.1$ Hz, 4-Hpy(OMe)). FT-IR (CH$_2$Cl$_2$): $\nu$(CO) 2093 cm$^{-1}$.

**[L$^3$Cu(PPh$_3$)](OTf).** Colorless cubic crystals suitable for X-ray analysis are grown from a solution of the complex in acetone layered with hexanes. $^1$H NMR (400 MHz, acetone-$d_6$): 3.37 (9 H, s, py-OMe), 3.48 (3 H, s, C−OMe), 6.88 (3 H, d, $J = 8.4$ Hz, 5-Hpy(OMe)), 7.25−7.65 (15 H, m, Ph), 7.58 (3 H, d, $J = 7.6$ Hz, 3-Hpy(OMe)), 7.90 (3 H, t, $J = 7.8$ Hz, 4-Hpy(OMe)).

**Syntheses of Metal Complexes [(L)$_2$Cu$^I$](OTf).** The bis-ligated Cu(I) complexes are synthesized in acetone with 2 equiv of ligand, **L** (**L** = **L$^{0\rightarrow2}$**), and 1 equiv of [Cu$^I$(CH$_3$CN)$_4$](OTf). The products are isolated as orange powders from acetone/hexanes, and yields are nearly quantitative based on inspection of the $^1$H NMR spectra.

**[(L$^0$)$_2$Cu](OTf).** Yellow cubic crystals suitable for X-ray analysis are obtained by the slow evaporation of an acetone solution of the complex. $^1$H NMR (200 MHz, CDCl$_3$): 3.12 (3 H, br s, C−OMe), 7.21 (3 H, br t, $J = 4.0$ Hz, 5-Hpy), 7.46 (3 H, br d, 6-Hpy), 7.78 (3 H, br t, $J = 2.6$ Hz, 4-Hpy), 7.92 (3 H, d, $J = 5.0$ Hz, 3-Hpy). Elem. anal. Calcd for $C_{35}H_{30}N_6O_5F_3SCu$: C, 54.79; H, 3.94; N, 10.95. Found: C, 54.43; H, 3.74; N, 10.66.

**[(L$^1$)$_2$Cu](OTf).** Deep orange crystals suitable for X-ray analysis are obtained by an acetone solution of the complex layered with hexanes. $^1$H NMR (200 MHz, CDCl$_3$): 3.16 (3 H, s, C−OMe), 3.61 (3 H, s, py-OMe), 6.42 (1 H, d, $J = 7.6$ Hz, 3-Hpy(OMe)), 6.67 (1 H, d, $J = 8.2$ Hz, 5-Hpy(OMe)), 7.17 (2 H, br t, $J = 5.0$ Hz, 5-Hpy), 7.50 (2 H, br d, $J = 3.0$ Hz, 6-Hpy), 7.90 (1 H, t, $J = 9.8$ Hz, 4-Hpy(OMe)), 7.65 (2 H, t, $J = 1.6$ Hz, 4-Hpy), 8.08 (2 H, d, $J = 8.0$ Hz, 3-Hpy).

**[(L$^2$)$_2$Cu](OTf).** Orange prismatic crystals suitable for X-ray analysis are obtained by diffusion of hexanes into an acetone solution of the complex. $^1$H NMR (200 MHz, CDCl$_3$): 3.15 (3 H, s, C−OMe), 3.34 (3 H, s, py-OMe), 6.66 (2 H, d, $J = 7.8$ Hz, 5-Hpy(OMe)), 7.01 (2 H, d, $J = 6.0$ Hz, 3-Hpy(OMe)), 7.03 (1 H, br t, 5-Hpy), 7.46 (1 H, br d, $J = 3.2$ Hz, 6-Hpy), 7.70 (2 H, t, $J = 6.8$ Hz, 4-Hpy(OMe)), 7.79 (1 H, t, $J = 8.2$ Hz, 4-Hpy), 7.94 (1 H, d, $J = 8.0$ Hz, 3-Hpy). Elem. anal. Calcd for $C_{39.5}H_{41}N_6O_{6.5}F_3SCu$: C, 53.08; H, 4.51; N, 9.17. Found: C, 52.99; H, 4.49; N, 8.98.

**Syntheses of Metal Complexes [(L)$_2$Cu$^{II}$](OTf)$_2$.** The bis-ligated Cu(II) complexes are synthesized directly in acetone with 2 equiv of ligand, **L** (**L** = **L$^{0\rightarrow3}$**), and 1 equiv of Cu$^{II}$(OTf)$_2$ in nearly quantitative yield. These complexes may also be isolated from disproportionation of the [**L**Cu$^I$(CH$_3$CN)](OTf) complexes in acetone for all but the **L** = **L$^3$** complex, with yields approaching 50%. The products were isolated as blue to green crystalline powders after removal of the solvent.

**[(L$^0$)$_2$Cu](OTf)$_2$.** X-ray-quality blue block-shaped crystals are obtained upon standing of a concentrated solution of the complex in acetone. Absorption spectrum (CH$_2$Cl$_2$): $\lambda_{max}$ (nm), $\epsilon$ (M$^{-1}$ cm$^{-1}$); 588, 27. EPR (CH$_2$Cl$_2$ glass): $g_{||} = 2.228$, $A_{||}$ (gauss) = 181. Elem. anal. Calcd for $C_{36}H_{30}N_6O_8F_6S_2Cu$: C, 47.19; H, 3.30; N, 9.17. Found: C, 47.01; H, 3.23; N, 9.04.

**[(L$^1$)$_2$Cu](OTf)$_2$.** X-ray-quality blue/green block-shaped crystals are obtained from an ether-layered CH$_3$CN solution of the complex. Absorption spectrum (CH$_2$Cl$_2$): $\lambda_{max}$ (nm), $\epsilon$ (M$^{-1}$ cm$^{-1}$); 580, 57. EPR (CH$_2$Cl$_2$ glass): $g_{||} = 2.224$, $A_{||}$ (gauss) = 184.

**[(L$^2$)$_2$Cu](OTf)$_2$.** X-ray-quality blue prismatic crystals are obtained from a CH$_2$Cl$_2$/ether solution of the complex. Absorption spectrum (CH$_2$Cl$_2$): $\lambda_{max}$ (nm), $\epsilon$ (M$^{-1}$ cm$^{-1}$); 620, 37. EPR (CH$_2$Cl$_2$ glass): $g_{||} = 2.253$, $A_{||}$ (gauss) = 168.

**[(L$^3$)$_2$Cu](OTf)$_2$.** X-ray-quality green cubic crystals are obtained from an ether-layered acetone solution of the complex. Absorption spectrum (CH$_2$Cl$_2$): $\lambda_{max}$ (nm), $\epsilon$ (M$^{-1}$ cm$^{-1}$); 686, 32. EPR (CH$_2$Cl$_2$ glass): $g_{||} = 2.293$, $A_{||}$ (gauss) = 150.

**[L$^3$Cu(H$_2$O)$_3$](OTf)$_2$.** Exposure of [(**L$^3$**)$_2$Cu](OTf)$_2$ to atmospheric moisture results in the formation of the tris-aqua species, [**L$^3$**Cu(H$_2$O)$_3$](OTf)$_2$. X-ray-quality blue/green cubic crystals are obtained by slow evaporation of a CH$_2$Cl$_2$/ether solution of the complex. Absorption Spectrum (CH$_2$Cl$_2$): $\lambda_{max}$ (nm), $\epsilon$ (M$^{-1}$ cm$^{-1}$); 640, 25. EPR (CH$_2$Cl$_2$ glass): $g_{||} = 2.291$, $A_{||}$ (gauss) = 168. Elem. anal. Calcd for $C_{22}H_{27}N_3O_{13}F_6S_2Cu$: C, 33.74; H, 3.48; N, 5.37. Found: C, 33.87; H, 3.24; N, 6.01.

**X-ray Crystallography. General Methods.** For each of the X-ray crystal structures presented, the data set was collected at a temperature of −70 °C using the $\omega$ scan technique. A suitably sized crystal was mounted in paratone oil on a glass fiber and placed in a cold stream of nitrogen on an Enraf-Nonius CAD-4 diffractometer with graphite monochromatic Mo K$\alpha$ radiation ($\lambda$ = 0.710 73 Å). Unit cell parameters and an orientation matrix were typically obtained from 25 carefully centered reflections with 2$\theta$ near 36°. Important data collection and crystal parameters for the Cu(I) and Cu(II) structures are summarized in Tables 1 and 2, respectively. Moving-crystal, moving-counter background measurements were made by scanning an additional 25% above and below the scan range. The counter aperture consisted of a variable horizontal slit with a width ranging from 2.0 to 2.5 mm and a vertical slit set to 2.0 mm. Three intensity-check reflections were monitored hourly to determine the crystal decay due to X-ray exposure. For most of the data sets, a linear correction factor was applied. An empirical absorption correction based on azimuthal scans of several appropriate reflections was applied to all of the data sets. The data were corrected for Lorentz and polarization effects. The structures were all solved by direct methods[33] and expanded using Fourier techniques.[34] All non-hydrogen atoms were refined anisotropically, unless noted. Hydrogen atoms were located by difference Fourier maps but were included at idealized positions 0.95 Å from their parent atom for the final refinement. Isotropic thermal parameters 1.2 times the parent atom were assumed. Unless otherwise noted, the remaining significant peaks on the final difference Fourier map were located near the triflate anion(s). Neutral atom scattering factors were taken from Cromer and Waber.[35] Anomalous dispersion effects were included in $F_{calc}$;[36] the values for $\Delta f'$ and $\Delta f''$ were those of Creagh and McAuley.[37] The values for the mass attenuation coefficients are those of Creagh and Hubbell.[38] All calculations were performed using the teXsan[39] crystallographic software package from Molecular Structure Corporation. Specific details for each of the crystal structures are found in the following sections. For each structure the following information is available in the Supporting Information: an ORTEP representation of the cation(s) with complete labeling scheme, a packing diagram of the unit cell, a complete set of crystallographic tables including positional parameters, bond lengths, bond angles, and anisotropic thermal factors.

**[$L^0$Cu($CH_3CN$)](OTf).** Since the complex completely disproportionates in solution within a week, only weakly diffracting crystals could be obtained. The asymmetric unit contains one cation and one triflate anion. An ORTEP representation of the cation is shown in Figure 1a, and selected bond lengths and angles are presented in Table 3.

**[$L^3$Cu($CH_3CN$)](OTf).** The crystals are indefinitely stable in an inert atmosphere, but slowly decomposed in air to include a Cu(II) complex with similar characterization to the tris-squa species, [**L**$^3$Cu($H_2O$)$_3$](OTf)$_2$. Two independent cations are found in the asymmetric unit along with two triflate anions. One of the triflates is significantly disordered and was modeled with 2 rigid groups in a 30:70 ratio. All atoms in the rigid groups had their own isotropic thermal parameters. The maximum and minimum peaks on the final difference Fourier map corresponded to 0.88 and −0.73 e/Å$^3$, respectively, and were located near the disordered triflate anion. ORTEP representations of the two cations are shown in Figure 1b and c, and selected bond lengths and angles are presented in Table 3.

**[$L^1$Cu($PPh_3$)](OTf).** The asymmetric unit consists of one cation and one triflate anion. An ORTEP representation of the cation is shown in Figure 2a, and selected bond lengths and angles are presented in Table 4.

**[$L^3$Cu($PPh_3$)](OTf)·$^1/_2$(acetone).** Two independent cations, two triflate anions, and two half-occupancy acetone molecules comprise the asymmetric unit. One acetone molecule is disordered. The remaining significant peaks on the final difference Fourier map were located near the disordered solvent molecule. ORTEP representations of the two cations are shown in Figure 2b and c, and selected bond lengths and angles are presented in Table 4.

**[($L^0$)$_2$Cu](OTf)·(acetone).** The crystals are air stable for weeks before becoming dulled with slight green discoloration. The asymmetric unit consists of one cation, one triflate anion, and one acetone molecule. The assignment of the nitrogen atoms in the nonbinding pyridine rings was made with consideration of the $B_{iso}$ values for the two possible positions; the nitrogen atoms were assigned to minimize the $B_{iso}$ values. An ORTEP representation of the cation is shown in Figure 3a, and selected bond lengths and angles are presented in Table 3.

**[($L^1$)$_2$Cu](OTf).** The asymmetric unit contains two independent cations and two triflate anions. One triflate is disordered, and the carbon atom of this triflate was refined isotropically. The maximum and minimum peaks on the final difference Fourier map corresponded to 1.44 and −1.41 e/Å$^3$, respectively, and were located near the disordered triflate anion. ORTEP representations of the two cations are shown in Figure 3b and c, and selected bond lengths and angles are presented in Table 3.

**[($L^2$)$_2$Cu](OTf)·$^1/_2$(acetone).** The asymmetric unit consists of one cation, one triflate anion, and a half-occupancy acetone molecule. The acetone molecule is disordered over the crystallographic inversion center, and was modeled as two half-occupancy fragments. The packing diagram reveals the interaction of the fragments to give two half-occupancy acetone molecules. An ORTEP representation of the cation is shown in Figure 3d, and selected bond lengths and angles are presented in Table 3.

**[($L^0$)$_2$Cu](OTf)$_2$.** The copper atom resides on a crystallographic inversion center, so that the unit cell contains a single "bis-tris" Cu(II) cation and two triflate anions. An ORTEP representation of the cation is shown in Figure 4a, and selected bond lengths and angles are presented in Table 5.

**[($L^1$)$_2$Cu](OTf)$_2$·($CH_3CN$).** The copper atom resides on a crystallographic inversion center, so that the unit cell contains a single "bis-tris" Cu(II) cation, two triflate anions, and one $CH_3CN$ molecule. The maximum and minimum peaks on the final difference Fourier map corresponded to 0.46 and −0.36 e/Å$^3$, respectively, and were located near the $CH_3CN$ molecule. An ORTEP representation of the cation is shown in Figure 4b, and selected bond lengths and angles are presented in Table 5.

**[($L^2$)$_2$Cu](OTf)$_2$.** The copper atom resides on a crystallographic inversion center, so that the unit cell contains a single "bis-tris" Cu(II) cation and two triflate anions. While one methoxypyridine of each ligand is bound in the axial position, the other methoxypyridine is disordered over the two equatorial positions. Both equatorial Cu(II) binding groups were modeled as methoxypyridines, with the occupancy of these methoxy groups set at 50%. The maximum and minimum peaks on the final difference Fourier map corresponded to 1.92 and −1.33 e/Å$^3$, respectively. Some of the highest remaining peaks were associated with one of the methoxy groups. The remaining significant peaks were located near the triflate anions. An ORTEP representation of the cation with one set of methoxy groups at 100% occupancy is shown in Figure 4c, and selected bond lengths and angles are presented in Table 5.

**[($L^3$)$_2$Cu](OTf)$_2$·(acetone).** Over the course of data collection, the intensity standards decreased by an average of 17.5%. After about a third of the reflections had been measured, the crystal shifted, resulting in a sudden sharp decrease in the intensity standards, which then assumed a linear decay. A polynomial correction factor was applied to the data to account for this phenomenon. The asymmetric unit consists of one cation, two triflate anions, and one acetone molecule. Both triflate anions are disordered. The maximum and minimum peaks on the final difference Fourier map corresponded to 1.04 and −0.87 e/Å$^3$, respectively, and were located near the disordered triflate anions. An ORTEP representation of the cation is shown in Figure 5a, and selected bond lengths and angles are presented in Table 5.

---

(33) Fan, H.-F. *SAPI91: Structure Analysis Programs with Intelligent Control*; Rigaku Corporation; Tokyo, Japan, 1991.

(34) Beurskens, P. T.; Admiraal, G.; Beurskens, G.; Bosman, W. P.; Garcia-Granda, S.; Gould, R. O.; Smits, J. M. M.; Smykalla, C. *DIRDIF92: The DIRDIF Program System*; Technical Report of the Crystallography Laboratory: University of Nijmegen, The Netherlands, 1992.

(35) Cromer, D. T.; Waber, J. T. *International Tables for X-ray Crystallography*; The Kynoch Press: Birmingham, 1974; Vol. IV.

(36) Ibers, J. A.; Hamilton, W. C. *Acta Crystallogr.* **1964**, *17*, 781.

(37) Creagh, D. C.; McAuley, W. J. In *International Tables for Crystallography*; Wilson, A. J. C., Ed.; Kluwer Academic Publishers: Boston, 1992; Vol. C, Table 4.2.6.8, pp 219−220.

(38) Creagh, D. C.; Hubbell, J. H. In *International Tables for Crystallography*; Wilson, A. J. C., Ed.; Kluwer Academic Publishers: Boston, 1992; Vol. C, Table 4.2.4.3, pp 200−206.

(39) *teXsan: Texray Crystal Structure Analysis Package*; Molecular Structure Corp.: The Woodlands, TX, 1992.

**Table 1.** Summary of Crystallographic Data of Cu(I) Complexes

| compound | $[\mathbf{L^0}Cu(CH_3CN)](OTf)$ | $[\mathbf{L^3}Cu(CH_3CN)](OTf)$ | $[\mathbf{L^1}Cu(PPh_3)](OTf)$ | $[\mathbf{L^3}Cu(PPh_3)](OTf)\cdot{}^1/_2(acetone)$ | $[(\mathbf{L^0})_2Cu](OTf)\cdot(acetone)$ | $[(\mathbf{L^1})_2Cu](OTf)$ | $[(\mathbf{L^2})_2Cu](OTf)\cdot{}^1/_2(acetone)$ |
|---|---|---|---|---|---|---|---|
| formula | $C_{20}H_{18}N_4O_4F_3SCu$ | $C_{23}H_{24}N_4O_7F_3SCu$ | $C_{37}H_{32}N_3O_5F_3PSCu$ | $C_{40.5}H_{39}N_3O_{7.5}F_3PSCu$ | $C_{38}H_{36}N_6O_6F_3SCu$ | $C_{37}H_{34}N_6O_7F_3SCu$ | $C_{40.5}H_{41}N_6O_{9.5}F_3SCu$ |
| fw | 530.99 | 621.07 | 782.25 | 871.33 | 825.34 | 827.31 | 914.89 |
| temperature (K) | 203 | 203 | 203 | 203 | 203 | 203 | 203 |
| crystal system | monoclinic | triclinic | triclinic | triclinic | monoclinic | monoclinic | triclinic |
| space group | $P2_1/c$ (No. 14) | $P1$ (No. 1) | $P\bar{1}$ (No. 2) | $P\bar{1}$ (No. 2) | $P2_1/a$ (No. 14) | $P2_1/n$ (No. 14) | $P\bar{1}$ (No. 2) |
| $a$ (Å) | 8.265(1) | 8.115(1) | 10.422(2) | 14.855(5) | 16.778(1) | 20.277(2) | 12.509(4) |
| $b$ (Å) | 13.784(7) | 11.556(1) | 11.860(2) | 16.613(5) | 13.970(2) | 15.179(2) | 12.716(4) |
| $c$ (Å) | 19.397(3) | 14.032(1) | 15.877(3) | 17.129(6) | 16.940(2) | 24.283(2) | 14.889(5) |
| α (deg) | 90.00 | 87.877(6) | 73.44(1) | 78.01(3) | 90.00 | 90.00 | 103.11(3) |
| $\beta$ (deg) | 97.168(9) | 88.084(5) | 81.32(1) | 85.02(3) | 113.583(7) | 98.297(6) | 110.08(3) |
| $\gamma$ (deg) | 90.00 | 84.762(6) | 69.14(1) | 89.19(3) | 90.00 | 90.00 | 102.78(3) |
| volume (Å$^3$) | 2192(1) | 1308.8(2) | 1755.1(6) | 4119(2) | 3638.8(7) | 7395(1) | 2047(1) |
| $Z$ | 4 | 2 | 2 | 4 | 4 | 8 | 2 |
| $\mu_{calc}$ (cm$^{-1}$) | 11.52 | 9.86 | 7.91 | 6.88 | 7.30 | 7.21 | 6.63 |
| $F_{000}$ | 1080 | 636 | 804 | 1816 | 1704 | 3408 | 945 |
| $\rho_{obs}$ ($\rho_{calc}$) (g cm$^{-3}$) | >1.594 (1.609) | 1.563 (1.576) | 1.44 (1.480) | 1.398 (1.396) | 1.494 (1.506) | 1.475 (1.488) | 1.467 (1.484) |
| crystal size (mm) | 0.30 × 0.40 × 0.20 | 0.60 × 0.80 × 0.60 | 0.60 × 0.50 × 0.10 | 0.30 × 0.30 × 0.20 | 0.50 × 0.60 × 0.20 | 0.40 × 0.40 × 0.20 | 0.40 × 0.30 × 0.30 |
| radiation | Mo Kα | Mo Kα | Mo Kα | Mo Kα | Mo Kα | Mo Kα | Mo Kα |
| no. of reflcns measd | $(+h, +k, \pm l)$ | $(+h, \pm k, \pm l)$ | $(+h, \pm k, \pm l)$ | $(+h, \pm k, \pm l)$ | $(+h, +k, \pm l)$ | $(+h, +k, \pm l)$ | $(+h, \pm k, \pm l)$ |
| $2\theta$ range | $10.0° < 2\theta < 50.0°$ | $10.0° < 2\theta < 50.0°$ | $10.0° < 2\theta < 50.0°$ | $10.0° < 2\theta < 46.8°$ | $10.0° < 2\theta < 50.0°$ | $10.0° < 2\theta < 50.0°$ | $10.0° < 2\theta < 50.0°$ |
| scan type | $\omega$ | $\omega$ | $\omega$ | $\omega$ | $\omega$ | $\omega$ | $\omega$ |
| scan width (deg) | $1.06 + 0.73 \tan\theta$ | $0.78 + 0.82 \tan\theta$ | $0.83 + 0.74 \tan\theta$ | $0.54 + 0.92 \tan\theta$ | $0.60 + 0.68 \tan\theta$ | $0.73 + 0.57 \tan\theta$ | $0.71 + 0.73 \tan\theta$ |
| scan speed ($\theta$, deg/min) | 5.5 | 5.5 | 5.5 | 5.5 | 5.4 | 5.5 | 5.5 |
| decay cor | linear | linear | linear | linear | linear | linear | linear |
| empirical abs cor | 0.77 to 1.00 | 0.77 to 1.00 | 0.79 to 1.00 | 0.88 to 1.00 | 0.91 to 1.00 | 0.92 to 0.99 | 0.97 to 1.00 |
| no. of reflcns collcd | 3636 | 4791 | 6506 | 14091 | 6906 | 11619 | 7532 |
| no. of unique reflcns | 3394 ($R_{int} = 0.103$) | 4586 ($R_{int} = 0.0507$) | 6152 ($R_{int} = 0.0275$) | 12041($R_{int} = 0.0572$) | 6714 ($R_{int} = 0.0434$) | 11386 ($R_{int} = 0.0489$) | 7176 ($R_{int} = 0.0236$) |
| no. of reflcns with ($F_o^2 > 3.00\sigma(F_o^2)$) | 1772 | 4390 | 4496 | 7560 | 3869 | 5092 | 5301 |
| no. of parameters | 298 | 680 | 460 | 1019 | 496 | 986 | 559 |
| refl/param ratio | 5.95 | 6.46 | 9.77 | 7.42 | 7.80 | 5.16 | 9.48 |
| $R$ ($R_w$)[a] | 0.052 (0.047) | 0.049 (0.065) | 0.049 (0.060) | 0.052 (0.062) | 0.041 (0.036) | 0.072 (0.068) | 0.062 (0.091) |
| final diff $\rho_{max}$ (e/Å$^3$) | +0.59; −0.53 | +0.88; −0.73 | +0.80; −0.58 | +0.95; −0.52 | +0.54; −0.49 | +1.44; −1.41 | +0.67; −0.67 |

[a] $R = \sum||F_o| - |F_c||/\sum|F_o|$; $[\sum w(|F_o| - |F_c|)^2/\sum wF_o^2]^{1/2}$, where $w = 4F_o^2/\sigma^2(F_o^2)$; $\sigma^2(F_o^2) = S^2(C + R^2B) + (pF_o^2)^2/(Lp)^2$ with $S$ = scan rate, $C$ = total integrated peak count, $R$ = ratio of scan time to background counting time, $B$ = total background count, $Lp$ = Lorentz polarization factor, $p$ = $p$ factor {0.011 for $[\mathbf{L^0}Cu(CH_3CN)](OTf)_2$, 0.019 for $[\mathbf{L^3}Cu(CH_3CN)](OTf)$, 0.030 for $[\mathbf{L^1}Cu(PPh_3)](OTf)$, 0.014 for $[\mathbf{L^3}Cu(PPh_3)](OTf)\cdot{}^1/_2(acetone)$, 0.007 for $[(\mathbf{L^0})_2Cu](OTf)\cdot(acetone)$, 0.008 for $[(\mathbf{L^1})_2Cu](OTf)$, and 0.031 for $[(\mathbf{L^2})_2Cu](OTf)\cdot{}^1/_2(acetone)$}.

**Table 2.** Summary of Crystallographic Data of Cu(II) Complexes

| compound | $[(\mathbf{L}^0)_2\mathrm{Cu}](\mathrm{OTf})_2$ | $[(\mathbf{L}^1)_2\mathrm{Cu}](\mathrm{OTf})_2\cdot(\mathrm{CH_3CN})$ | $[(\mathbf{L}^2)_2\mathrm{Cu}](\mathrm{OTf})_2$ | $[(\mathbf{L}^3)_2\mathrm{Cu}](\mathrm{OTf})_2\cdot$(acetone) | $[\mathbf{L}^3\mathrm{Cu(H_2O)_3}](\mathrm{OTf})_2\cdot(\mathrm{H_2O})$ |
|---|---|---|---|---|---|
| formula | $C_{36}H_{30}N_6O_8F_6S_2Cu$ | $C_{40}H_{37}N_7O_{10}F_6S_2Cu$ | $C_{40}H_{36}N_6O_{12}F_6S_2Cu$ | $C_{45}H_{48}N_6O_{15}F_6S_2Cu$ | $C_{22}H_{29}N_3O_{14}F_6S_2Cu$ |
| fw | 916.32 | 1017.41 | 1034.41 | 1154.56 | 801.14 |
| temperature (K) | 203 | 203 | 203 | 203 | 203 |
| crystal system | triclinic | triclinic | triclinic | monoclinic | triclinic |
| space group | $P\bar{1}$ (No. 2) | $P\bar{1}$ (No. 2) | $P\bar{1}$ (No. 2) | $P2_1/n$ (No. 14) | $P\bar{1}$ (No. 2) |
| *a* (Å) | 8.574(1) | 9.663(1) | 10.027(2) | 14.949(7) | 9.266(1) |
| *b* (Å) | 10.336(1) | 9.822(1) | 10.948(1) | 20.54(1) | 13.205(2) |
| *c* (Å) | 11.794(1) | 12.949(2) | 11.541(1) | 16.461(7) | 14.563(1) |
| α (deg) | 73.581(6) | 70.31(1) | 72.799(9) | 90.00 | 107.060(8) |
| *β* (deg) | 68.071(6) | 72.87(1) | 74.45(1) | 96.02(4) | 97.336(6) |
| *γ* (deg) | 86.244(6) | 87.037(9) | 86.11(1) | 90.00 | 108.075(8) |
| volume ($Å^3$) | 929.1(2) | 1104.2(3) | 1165.9(3) | 5026(3) | 1571.8(4) |
| Z | 1 | 1 | 1 | 4 | 2 |
| $\mu_{calc}$ ($cm^{-1}$) | 7.92 | 6.79 | 6.47 | 6.13 | 9.3 |
| $F_{000}$ | 467 | 527 | 529 | 2380 | 818 |
| $\rho_{obs}$ ($\rho_{calc}$) (g $cm^{-3}$) | >1.594 (1.638) | 1.534 (1.539) | 1.454 (1.473) | 1.544 (1.525) | >1.594 (1.693) |
| crystal size (mm) | 0.50 × 0.30 × 0.30 | 0.20 × 0.40 × 0.50 | 0.70 × 0.50 × 0.40 | 0.60 × 0.50 × 0.40 | 0.50 × 0.50 × 0.10 |
| radiation | Mo Kα | Mo Kα | Mo Kα | Mo Kα | Mo Kα |
| reflcns measd | $(+h, \pm k, \pm l)$ | $(+h, \pm k, \pm l)$ | $(+h, \pm k, \pm l)$ | $(+h, +k, \pm l)$ | $(+h, \pm k, \pm l)$ |
| 2*θ* range | $10.0° < 2\theta < 50.0°$ | $10.0° < 2\theta < 50.0°$ | $11.0° < 2\theta < 50.0°$ | $10.0° < 2\theta < 50.0°$ | $8.2° < 2\theta < 49.9°$ |
| scan type | *ω* | *ω* | *ω* | *ω* | *ω* |
| scan width (deg) | $0.73 + 0.75 \tan \theta$ | $0.98 + 0.62 \tan \theta$ | $1.38 + 0.67 \tan \theta$ | $0.54 + 0.64 \tan \theta$ | $0.72 + 0.71 \tan \theta$ |
| scan speed (*θ*, deg/min) | 5.5 | 5.5 | 5.5 | 5.5 | 5.5 |
| decay cor | linear | linear | linear | polynomial | linear |
| empirical abs cor | 0.92 to 1.00 | 0.90 to 1.00 | 0.86 to 1.00 | 0.88 to 1.00 | 0.79 to 1.00 |
| no. of reflcns collcd | 3423 | 4057 | 4312 | 9450 | 5770 |
| no. of unique reflcns | 3249 ($R_{int} = 0.0129$) | 3874 ($R_{int} = 0.0182$) | 4081 ($R_{int} = 0.0133$) | 9224 ($R_{int} = 0.0348$) | 5507 ($R_{int} = 2.17$) |
| no. of reflections with ($F_o^2 > 3.00\sigma(F_o^2)$) | 2889 | 3049 | 3238 | 5919 | 4244 |
| no. of parameters | 268 | 313 | 311 | 676 | 433 |
| refl/param ratio | 10.78 | 9.74 | 10.41 | 8.76 | 9.80 |
| $R$ ($R_w$)[a] | 0.038 (0.049) | 0.038 (0.042) | 0.088 (0.106) | 0.058 (0.062) | 0.047 (0.055) |
| final diff $\rho_{max}$ (e/$Å^3$) | +0.58; −0.57 | +0.46; −0.36 | +1.92; −1.33 | +1.04; −0.87 | +0.87; −0.84 |

[a] $R = \sum||F_o| - |F_c||/\sum|F_o|$; $R_w = [\sum w(|F_o| - |F_c|)^2/\sum wF_o^2]^{1/2}$, where $w = 4F_o^2/\sigma^2(F_o^2)$; $\sigma^2(F_o^2) = S^2(C + R^2B) + (pF_o^2)^2/(Lp)^2$, with $S$ = scan rate, $C$ = total integrated peak count, $R$ = ratio of scan time to background counting time, $B$ = total background count, $Lp$ = Lorentz polarization factor, $p$ = $p$ factor {0.008 for $[(\mathbf{L}^0)_2\mathrm{Cu}](\mathrm{OTf})_2$, 0.014 for $[(\mathbf{L}^1)_2\mathrm{Cu}](\mathrm{OTf})_2\cdot(\mathrm{CH_3CN})$, 0.012 for $[(\mathbf{L}^2)_2\mathrm{Cu}](\mathrm{OTf})_2$, 0.010 for $[(\mathbf{L}^3)_2\mathrm{Cu}](\mathrm{OTf})_2\cdot$(acetone), and 0.016 for $[\mathbf{L}^3\mathrm{Cu(H_2O)_3}](\mathrm{OTf})_2\cdot(\mathrm{H_2O})$}.

**$[\mathbf{L}^3\mathbf{Cu(H_2O)_3}](\mathbf{OTf})_2\cdot(\mathbf{H_2O})$.** The asymmetric unit consists of one cation with three associated water ligands, two triflate anions, and a water molecule of solvation. The hydrogen atoms of the three water molecules bound to the Cu(II) center could be assigned by difference maps and hydrogen bonding interactions with the solvent water molecule and triflate anions. An ORTEP representation of the cation is shown in Figure 5b, and selected bond lengths and angles are presented in Table 5.

## Results and Discussion

**Ligand Syntheses.** Tris(2-pyridyl)carbinol (TPC) is a facial-capping, trinitrogen ligand which has rarely been used since its original synthesis. TPC was first characterized as a low-yield byproduct in the formation of bis(2-pyridyl)ketone from 2-pyridylmagnesium iodide and ethyl picolinate.[40] The overall yield of TPC has been increased to 25% by a stepwise synthesis of bis(2-pyridyl)ketone from 2-lithiopyridine and 2-cyanopyridine (40%), followed by nucleophilic attack of the ketone with 2-lithiopyridine (60%) (Scheme 1).[22,41] Synthesis of TPC using 3 equiv of 2-lithiopyridine with either ethylchloroformate or carbonyldiimidazole (CDI) also proceeds in extremely low yields (<10%). However, slightly greater yields result (30%) from the reaction of 2-lithiopyridine and picolinic acid chloride. As the bis(2-pyridyl)ketone starting material is commercially available, the synthetic procedure using 2-lithiopyridine remains the most efficient.

Our goal of developing a modular synthetic scheme to position functional groups at the periphery of the metal coordination site required derivatization of the 6-positions of the pyridyl subunits in TPC. A synthetically useful ketone with this substitution pattern, bis(2-(6-bromo)pyridyl)ketone, has been previously reported.[42] The yield of this ketone from 2-lithio-6-bromopyridine and ethylchloroformate was more than double that of the unsubstituted bis(2-pyridyl)ketone, revealing a potential synthetic advantage of 6-pyridyl substitutions in increasing product yield in lithio-reagent reactions. However, attempts to further convert this ketone into TPC derivatives via reactions with lithiopyridine reagents reveal that the 6-position with bromide substituents are vulnerable to nucleophilic attack. Only the bis(2-pyridyl)(2-(6-bromo)pyridyl)carbinol product, prepared from bis(2-pyridyl)ketone and 2-bromo-6-lithiopyridine, is isolated in a reasonable yield (50%).

A series of ligands has been prepared by introducing a variable number of methoxy groups at the 6-position of the pyridyl rings (Chart 1). The lithiopyridine precursor, 2-bromo-6-methoxypyridine, is readily synthesized[32] and used in the synthesis of the disubstituted ketone and the trisubstituted TPC ligands. Each of the four ligands in the series (0→3 OMe groups) was further modified by methylation of the bridgehead alcohol group to decrease its ability to act as a ligand. Previous studies have shown that TPC can adopt an *N*,*N*′,*O*(alkoxide) coordination mode with Co(II), instead of the desired facial-capping *N*,*N*′,*N*″ coordination mode.[43] Final yields of the three methoxy-substituted ligands proved to be much greater than the

---

(40) de Jonge, A. P.; den Hertog, H. J.; Wibaut, J. P. *Recl. Trav. Chim. Pays-Bas* **1951**, *70*, 989−996.

(41) Faller, J. W.; Ma, Y. *J. Am. Chem. Soc.* **1991**, *113*, 1579−1586.

(42) Parks, J. E.; Wagner, B. E.; Holm, R. H. *J. Organomet. Chem.* **1973**, *56*, 53−66.

(43) Szalda, D. J.; Keene, F. R. *Inorg. Chem.* **1986**, *25*, 2795−2799.

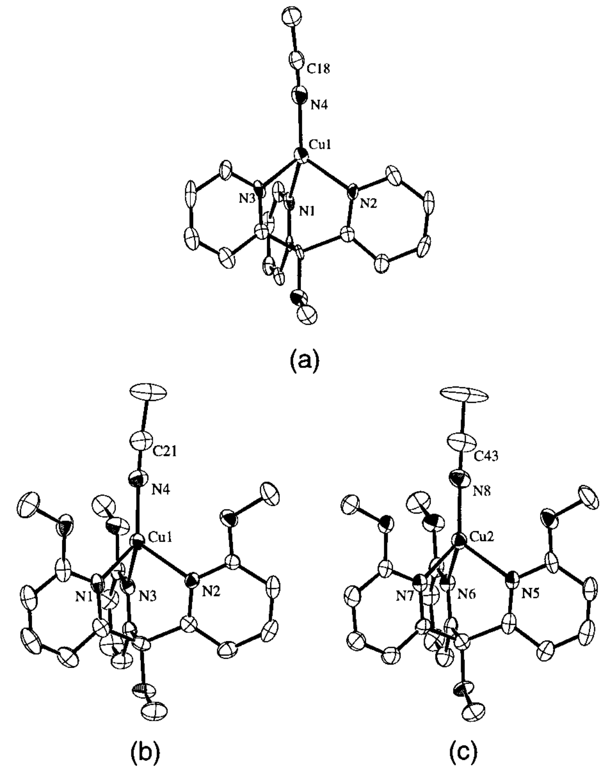

**Figure 1.** ORTEP representations (50% probability) without hydrogens nearly along the pseudo-mirror plane for (a) [$\mathbf{L^0}$Cu(CH$_3$CN)]$^+$ and (b and c) the two independent cations of [$\mathbf{L^3}$Cu(CH$_3$CN)]$^+$. The dihedral angles between pyridine planes as designated by their nitrogen label: [$\mathbf{L^0}$Cu(CH$_3$CN)]$^+$, N$_2$-N$_3$, 140°; N$_1$-N$_2$, 104°; N$_1$-N$_3$, 122°; (b) [$\mathbf{L^3}$Cu(CH$_3$CN)]$^+$, N$_1$-N$_2$, 145°; N$_2$-N$_3$, 106°; N$_1$-N$_3$, 108°; (c) [$\mathbf{L^3}$Cu(CH$_3$CN)]$^+$, N$_5$-N$_7$, 155°; N$_5$-N$_6$ 116°; N$_6$-N$_7$, 109°.

unsubstituted ligand, again showing the synthetic advantage of certain 6-pyridyl substituents in the preparation of these ligands.

**Metal Complex Syntheses.** The Cu(I) complexes are anaerobically synthesized from two different stoichiometric ratios of ligand and [Cu$^{\mathrm{I}}$(CH$_3$CN)$_4$](OTf) (OTf = CF$_3$SO$_3$$^-$). Pseudo-tetrahedral monomers with the general formula [$\mathbf{L}^{0\rightarrow3}$-Cu$^{\mathrm{I}}$(CH$_3$CN)](OTf) (where $\mathbf{L}^{0\rightarrow3}$ indicates the four complexes with ligands $\mathbf{L^0}$ through $\mathbf{L^3}$) result from an equimolar mixture of the reactants (eq 1). The CH$_3$CN ligand of [$\mathbf{L}^{0\rightarrow3}$Cu$^{\mathrm{I}}$(CH$_3$CN)]$^+$ is readily displaced by 1 equiv of triphenylphosphine (PPh$_3$) or 1 atm of carbon monoxide (CO). The CH$_3$CN monomers are isolated as moisture-sensitive, pale yellow crystalline solids, and the PPh$_3$ and CO complexes as colorless solids. Bis-ligated species of the formula [($\mathbf{L}^{0\rightarrow2}$)$_2$Cu](OTf) are synthesized from 2:1 ratios of ligand and Cu(I) (eq 2). These complexes are stable in solution in air for weeks. All the Cu(I) compounds are characterized by $^1$H NMR spectroscopy, and many by X-ray crystallography. The bis-ligated Cu(II) complexes, [($\mathbf{L}^{0\rightarrow3}$)$_2$Cu](OTf)$_2$, are prepared by reacting free ligand and Cu$^{\mathrm{II}}$(OTf)$_2$ in a 2:1 ratio to give nearly quantitative yields of blue to blue-green crystalline solids (eq 3). These complexes are characterized by X-ray crystallography, EPR spectroscopy, and UV/vis spectroscopy.

$$\mathbf{L}^{0\rightarrow3} + [\mathrm{Cu^I(CH_3CN)_4}](\mathrm{OTf}) \rightarrow [\mathbf{L}^{0\rightarrow3}\mathrm{Cu^I(CH_3CN)}](\mathrm{OTf}) \tag{1}$$

$$2\,\mathbf{L}^{0\rightarrow2} + [\mathrm{Cu^I(CH_3CN)_4}](\mathrm{OTf}) \rightarrow [(\mathbf{L}^{0\rightarrow2})_2\mathrm{Cu^I}](\mathrm{OTf}) \tag{2}$$

$$2\,\mathbf{L}^{0\rightarrow3} + \mathrm{Cu^{II}(OTf)_2} \rightarrow [(\mathbf{L}^{0\rightarrow3})_2\mathrm{Cu^{II}}](\mathrm{OTf})_2 \tag{3}$$

**Solid State Structures.** Seven Cu(I) and five Cu(II) complexes of the ligand series are characterized by X-ray crystallography. Two distinct coordination modes of Cu(I) are found: a monoligated pseudo-tetrahedral arrangement, [$\mathbf{L}^{0\rightarrow3}$-Cu(CH$_3$CN)]$^+$, and a bis-ligated tetradentate configuration, [($\mathbf{L}^{0\rightarrow2}$)$_2$Cu]$^+$. Structural characterization of the ligands with Cu(II) shows a familiar "bis-tris" configuration of facial-capping trinitrogen ligands with Cu(II), [($\mathbf{L}^{0\rightarrow2}$)$_2$Cu]$^{2+}$.[44] The copper(II) is ligated in an axially distorted octahedral coordination with four nearly equivalent equatorial Cu(II)−N(py) bond distances and two elongated axial Cu(II)−N(py) distances. A structurally characterized monoligated, tris-aqua species is also found with the most sterically encumbered ligand in the series, [$\mathbf{L^3}$Cu$^{\mathrm{II}}$(H$_2$O)$_3$](OTf)$_2$. Important data collection and crystal parameters for the Cu(I) and Cu(II) structures are summarized in Tables 1 and 2, respectively.

Two crystal structures of the formula [$\mathbf{L}$Cu(CH$_3$CN)](OTf) ($\mathbf{L}$ = $\mathbf{L^0}$, $\mathbf{L^3}$) have been determined. The asymmetric unit in the [$\mathbf{L^0}$Cu(CH$_3$CN)]$^+$ crystal contains one Cu(I)−ligand complex (Figure 1a), while the asymmetric unit in the [$\mathbf{L^3}$Cu(CH$_3$CN)]$^+$ crystal contains two crystallographically independent Cu(I)−ligand complexes (Figure 1b,c) which are effectively isostructural (RMS error for the non-hydrogen atoms = 0.22 Å). The coordination of each complex is pseudo-tetrahedral, with the three nitrogen atoms of the ligand binding in a facial-capping mode, and a fourth CH$_3$CN ligand. As anticipated, the copper is ligated in a pseudo $C_3$ symmetric geometry by the coordinating nitrogen atoms; the Cu−N(py) bond lengths and N(py)−Cu−N(py) bite angles are nearly equivalent (Table 3). However, the overall pseudosymmetry of each cation is much closer to $C_s$ with the symmetry plane containing a single pyridine subunit ($\mathbf{Py_{sym}}$), the copper atom, the bridgehead carbon, the bridgehead methoxy group, and the heteroatom of the monodentate ligand. This requires a trans relationship of the ligated $\mathbf{Py_{sym}}$ and the bridgehead methoxy group. An examination of most structures indicates that the bridgehead methoxy group plays an important role in determining the geometry of these complexes not originally anticipated. The positioning of the methyl of the bridgehead methoxy between the cleft of two non-$\mathbf{Py_{sym}}$ pyridine subunits significantly opens this dihedral angle (Figure 1), and generally results in a slight lengthening of the N($\mathbf{Py_{sym}}$)−Cu bond distance relative to the other N(py)-Cu distances. This reduction in symmetry from $C_3$ to $C_s$ is likely responsible for the slight off-axis binding of the CH$_3$CN ligands in [$\mathbf{L}$Cu(CH$_3$CN)]$^+$ ($\mathbf{L}$ = $\mathbf{L^0}$, $\mathbf{L^3}$). The N(py)−Cu−N(CH$_3$CN) bond angles range from 113 to 140° in these complexes,

---

[44] Bis-tris Cu(II) complexes with 3-fold symmetic ligands: (a) Bis(hydrotris(1-pyrazolyl)borate: Murphy, A.; Hathaway, B. J.; King, T. J. *J. Chem. Soc., Dalton Trans.* **1979**, 1646−1650. (b) Bis(*cis,cis*-1,3,5-triaminocyclohexane: Ammeter, J. H.; Bürgi, H. B.; Gamp, E.; Meyer-Sandrin, V.; Jensen, W. P. *Inorg. Chem.* **1979**, *18*, 733−750. (c) Bis(1,4,7-triazacyclononane-*N, N′N″*): Chaudhuri, P.; Oder, K.; Wieghardt, K.; Weiss, J.; Reedijk, J.; Hinrichs, W.; Wood, J.; Ozarowski, A.; Stratemaier, H.; Reinen, D. *Inorg. Chem.* **1986**, *25*, 2951−2958. (d) Bis(hydrotris(3,5-dimethyl-1-pyrazolyl)borate-*N,N′,N″*): Kitajima, N.; Moro-oka, Y.; Uchida, A.; Sasada, Y.; Ohashi, Y. *Acta Crystallogr., Sect. C* **1988**, *44*, 1876−1878. (e) 1,3,5-Triamino-1,3,5-trideoxy-*cis*-inositol: Hegetschweiler, K.; Gramlich, V.; Ghisletta, M.; Samaras, H. *Inorg. Chem.* **1992**, *31*, 2341−2346. (f) Bis(tris(pyrazol-1-yl)methane-*N,N′,N″*): Astley, T.; Gulbis, J. M.; Hitchman, M. A.; Tiekink, E. R. T. *J. Chem. Soc., Dalton Trans.* **1993**, 509−515. (g) Bis(hydrotris(1,2,4-triazolyl)borate-*N,N′,N″*): Janiak, C. *Chem. Ber.* **1994**, *127*, 1379−1385. (h) Bis(tris(2-pyridyl)methane): Astley, T.; Headlam, H.; Hitchman, M. A.; Keene, F. R.; Pilbrow, J.; Stratemeier, H.; Tiekink, E. R. T.; Zhong, Y. C. *J. Chem. Soc., Dalton Trans.* **1995**, 3809−3818. (i) Bis(tris(2-pyridyl)phosphine): Astley, T.; Ellis, P. J.; Freeman, H. C.; Hitchman, M. A.; Keene, F. R.; Tiekink, E. R. T. *J. Chem. Soc., Dalton Trans.* **1995**, 595−601.

**Table 3.** Selected Bond Distances (Å) and Angles (deg) for the Cuprous Complexes

| | | $[\mathbf{L}^3Cu(CH_3CN)](OTf)$ | | | |
|---|---|---|---|---|---|
| $[\mathbf{L}^0Cu(CH_3CN)](OTf)$ | | unit A | | unit B | |
| Cu1−N1 | 2.065(6) | Cu1−N1 | 2.052(6) | Cu2−N5 | 2.072(6) |
| Cu1−N2 | 2.044(6) | Cu1−N2 | 2.062(6) | Cu2−N6 | 2.128(6) |
| Cu1−N3 | 2.087(6) | Cu1−N3 | 2.157(6) | Cu2−N7 | 2.042(6) |
| Cu1−N4 | 1.864(8) | Cu1−N4 | 1.881(7) | Cu2−N8 | 1.889(7) |
| N1−Cu1−N2 | 90.3(2) | N1−Cu1−N2 | 87.3(2) | N5−Cu2−N6 | 89.7(2) |
| N1−Cu1−N3 | 89.8(2) | N1−Cu1−N3 | 88.4(2) | N5−Cu2−N7 | 86.9(2) |
| N2−Cu1−N3 | 88.9(2) | N2−Cu1−N3 | 88.2(2) | N6−Cu2−N7 | 87.3(2) |
| N1−Cu1−N4 | 140.1(3) | N1−Cu1−N4 | 132.5(3) | N5−Cu2−N8 | 126.1(3) |
| N2−Cu1−N4 | 121.1(3) | N2−Cu1−N4 | 125.4(3) | N6−Cu2−N8 | 120.1(3) |
| N3−Cu1−N4 | 112.9(3) | N3−Cu1−N4 | 121.9(3) | N7−Cu2−N8 | 133.6(3) |

| | | $[(\mathbf{L}^1)_2Cu](OTf)$ | | | |
|---|---|---|---|---|---|
| $[(\mathbf{L}^0)_2Cu](OTf)\cdot$(acetone) | | unit A | | unit B | |
| Cu1−N2 | 2.112(3) | Cu1−N2 | 2.119(9) | Cu2−N8 | 2.126(9) |
| Cu1−N3 | 2.012(3) | Cu1−N3 | 1.986(9) | Cu2−N9 | 1.956(8) |
| Cu1−N5 | 2.010(3) | Cu1−N5 | 2.079(9) | Cu2−N11 | 2.167(9) |
| Cu1−N6 | 2.096(3) | Cu1−N6 | 2.004(8) | Cu2−N12 | 1.967(8) |
| N2−Cu1−N3 | 88.8(1) | N2−Cu1−N3 | 89.5(4) | N8−Cu2−N9 | 93.8(3) |
| N2−Cu1−N5 | 115.6(1) | N2−Cu1−N5 | 112.3(4) | N8−Cu2−N11 | 99.4(3) |
| N2−Cu1−N6 | 113.5(1) | N2−Cu1−N6 | 106.3(3) | N8−Cu2−N12 | 106.0(3) |
| N3−Cu1−N5 | 136.9(1) | N3−Cu1−N5 | 107.9(4) | N9−Cu2−N11 | 105.1(3) |
| N3−Cu1−N6 | 112.5(1) | N3−Cu1−N6 | 150.3(3) | N9−Cu2−N12 | 152.8(3) |
| N5−Cu1−N6 | 90.6(1) | N5−Cu1−N6 | 89.5(4) | N11−Cu2−N12 | 90.0(3) |

| $[(\mathbf{L}^2)_2Cu](OTf)\cdot{}^1/_2$(acetone) | | | |
|---|---|---|---|
| Cu1−N2 | 2.148(5) | N2−Cu1−N3 | 90.3(2) |
| Cu1−N3 | 2.005(5) | N2−Cu1−N5 | 117.4(2) |
| Cu1−N5 | 2.154(5) | N2−Cu1−N6 | 104.3(2) |
| Cu1−N6 | 2.006(5) | N3−Cu1−N5 | 111.8(2) |
| | | N3−Cu1−N6 | 144.5(2) |
| | | N5−Cu1−N6 | 90.1(2) |

reflecting a significant deviation from the idealized bond angle of 125.3° required for $C_3$ symmetry.

When the $CH_3CN$ ligands in $[\mathbf{L}^{0\rightarrow3}Cu(CH_3CN)](OTf)$ are replaced with $PPh_3$, a pronounced distortion of the ligation of the Cu(I) center is found. Two crystal structures of $[\mathbf{L}Cu(PPh_3)](OTf)$ ($\mathbf{L} = \mathbf{L}^1, \mathbf{L}^3$) have been determined. The Cu(I) center in $[\mathbf{L}^1Cu(PPh_3)]^+$ retains a pseudo-tetrahedral coordination (Figure 2a); however, the single methoxypyridine N−Cu bond is significantly longer than the other two Cu−N distances, consistent with the increased bulk of $PPh_3$ relative to $CH_3CN$. Much more pronounced structural differences are observed in the $[\mathbf{L}^3Cu(PPh_3)]^+$ complex which crystallizes with two structurally distinct monomers (Figure 2b and c). The first retains the expected pseudo-tetrahedral structure except that the Cu−N(py) bonds are all significantly elongated relative to $[\mathbf{L}^1Cu(PPh_3)]^+$ (average Cu−N = 2.15 Å in $[\mathbf{L}^3Cu(PPh_3)]^+$ versus 2.07 Å in $[\mathbf{L}^1Cu(PPh_3)]^+$) at the expense of maintaining a normal Cu−P distance of ca. 2.17 Å. In the second monomer, the coordination mode of the metal is trigonal planar, with $\mathbf{L}^3$ chelating in only a bidentate fashion, and the third methoxypyridine subunit oriented away from the metal. The release of a single sterically demanding pyridine subunit allows a significant decrease in the Cu−N distances (average Cu−N = 2.04 Å).

As additional free ligand is added to solutions of $[\mathbf{L}^{0\rightarrow2}Cu(CH_3CN)](OTf)$ the $CH_3CN$ ligand is displaced to form a bis-ligated, distorted tetrahedral Cu(I) complex with the general formula $[(\mathbf{L}^{0\rightarrow2})_2Cu](OTf)$. Three bis-ligated complexes are structurally characterized (Figure 3). In these structures, each ligand chelates through the two least bulky pyridyl groups of the ligand, while the third pyridine subunit is rotated away from

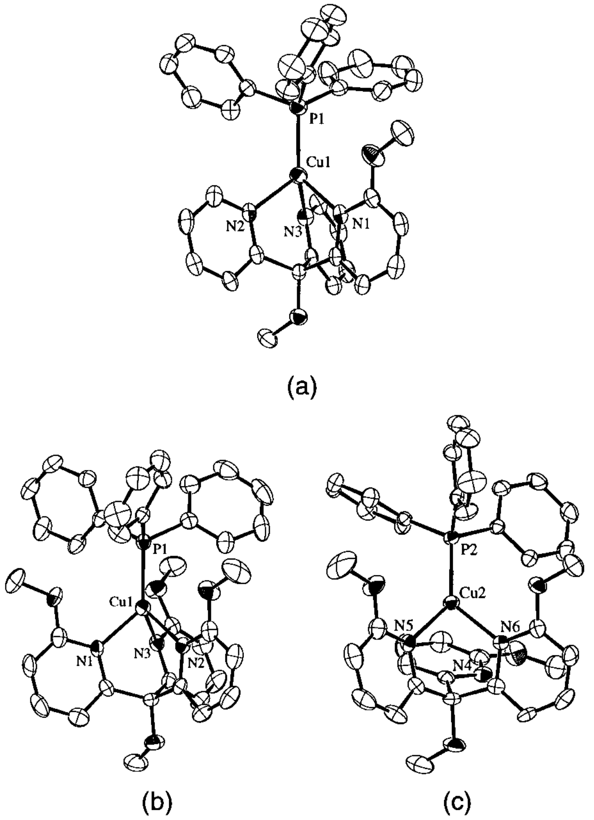

**Figure 2.** ORTEP representations (50% probability) without hydrogens for (a) $[\mathbf{L}^1Cu(PPh_3)]^+$, (b) the pseudo-tetrahedral cation of $[\mathbf{L}^3Cu(PPh_3)]^+$, and (c) the trigonal planar cation of $[\mathbf{L}^3Cu(PPh_3)]^+$.

**Table 4.** Selected Bond Distances (Å) and Angles (deg) for the $PPh_3$ Complexes

| | | [$\mathbf{L^3}$Cu($PPh_3$)](OTf) | | | |
|---|---|---|---|---|---|
| [$\mathbf{L^1}$Cu($PPh_3$)](OTf) | | pseudo-Td unit a | | trig planar unit b | |
| Cu1−N1 | 2.107(3) | Cu1−N1 | 2.040(5) | Cu2−N5 | 2.027(5) |
| Cu1−N2 | 2.039(3) | Cu1−N2 | 2.143(5) | Cu2−N6 | 2.055(5) |
| Cu1−N3 | 2.065(3) | Cu1−N3 | 2.140(5) | Cu2−P2 | 2.178(2) |
| Cu1−P1 | 2.160(1) | Cu1−P1 | 2.172(2) | | |
| N1−Cu1−N2 | 88.0(1) | N1−Cu1−N2 | 88.2(2) | N5−Cu2−N6 | 89.7(2) |
| N1−Cu1−N3 | 89.2(1) | N1−Cu1−N3 | 85.6(2) | N5−Cu2−P2 | 137.8(2) |
| N2−Cu1−N3 | 89.0(1) | N2−Cu1−N3 | 89.8(2) | N6−Cu2−P2 | 131.6(2) |
| N1−Cu1−P1 | 128.8(1) | N1−Cu1−P1 | 132.5(2) | | |
| N2−Cu1−P1 | 126.6(1) | N2−Cu1−P1 | 126.9(2) | | |
| N3−Cu1−P1 | 123.0(1) | N3−Cu1−P1 | 120.4(2) | | |

the copper and is nonligating. Comparison of the metrical parameters in Table 3 reveals that the [($\mathbf{L^{0\rightarrow 2}}$)$_2$Cu]$^+$ cations are effectively isostructural (RMS error for the non-hydrogen atoms = 0.25 Å). While the structures of [($\mathbf{L^0}$)$_2$Cu]$^+$ and [($\mathbf{L^2}$)$_2$Cu]$^+$ have a single cation in the asymmetric unit, the [($\mathbf{L^1}$)$_2$Cu]$^+$ complex contains two dissymmetric Cu(I) cations. The difference between the two independent cations occurs in the relative orientation of the noncoordinated methoxypyridine of each ligand. Though not crystallographically imposed, a pseudo-2-fold axis relates the two ligands in each structure. The escalation of the steric demands of the ligands does not effect the structural type of complex that can form until three methoxypyridines subunits are combined into a single ligand, $\mathbf{L^3}$. This ligand produces [$\mathbf{L^3}$Cu($CH_3CN$)]$^+$ in solution and solid state even under conditions of excess ligand (*vide infra*).

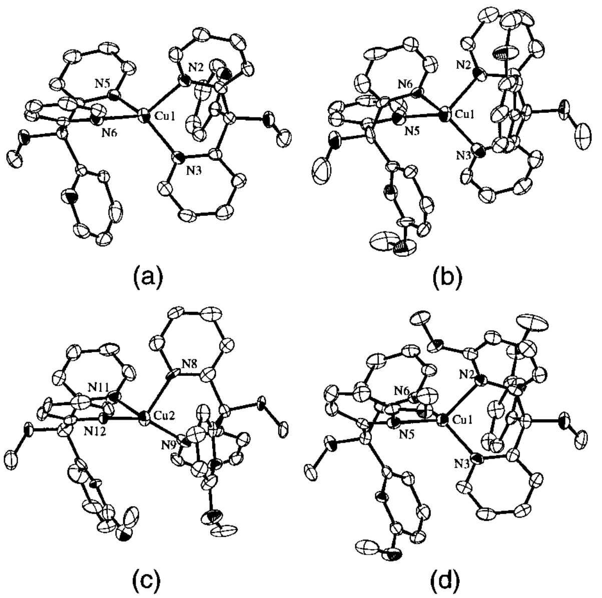

**Figure 3.** ORTEP representations (50% probability) without hydrogens for the cuprous complexes (a) [($\mathbf{L^0}$)$_2$Cu]$^+$, (b and c) the two independent cations of [($\mathbf{L^1}$)$_2$Cu]$^+$, and (d) [($\mathbf{L^2}$)$_2$Cu]$^+$.

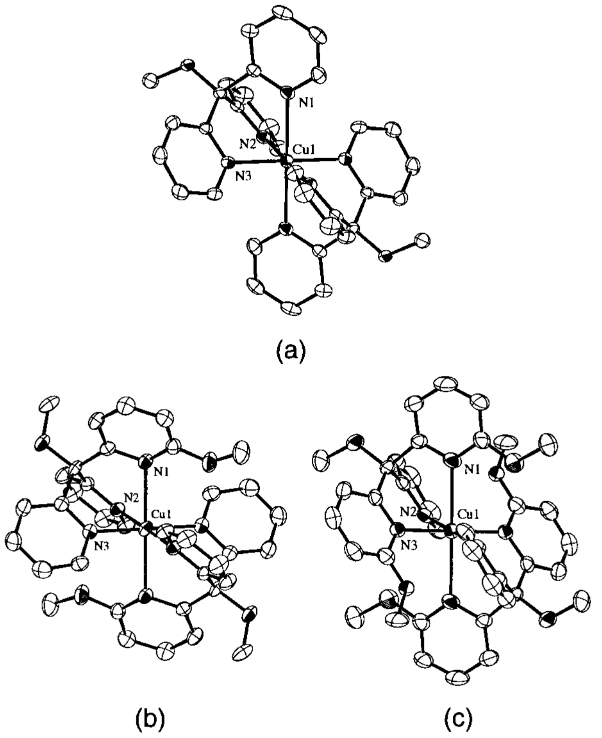

**Figure 4.** ORTEP representations (50% probability) without hydrogens for the cupric complexes (a) [($\mathbf{L^0}$)$_2$Cu]$^{2+}$, (b) [($\mathbf{L^1}$)$_2$Cu]$^{2+}$, and (c) [($\mathbf{L^2}$)$_2$Cu]$^{2+}$. The axial ligated nitrogen = N1 for all structures.

The Cu(I) structures indicate that the steric requirements of the ligands influence the observed geometric conformations. A similar conclusion can be drawn from the four "bis-tris" Cu(II) complexes that are formed. The [($\mathbf{L^{0\rightarrow 2}}$)$_2$Cu](OTf)$_2$ complexes are ligated in a tetragonally distorted octahedral coordination environment, with weakly bound axial ligation of the most bulky pyridine. ORTEP drawings of [($\mathbf{L^{0\rightarrow 2}}$)$_2$Cu]$^{2+}$ are shown in Figure 4, and selected metrical parameters are collected in Table 5. These three structures have imposed crystallographic inversion symmetry and, except for [($\mathbf{L^1}$)$_2$Cu]$^{2+}$, have the methoxy groups of the bridgehead carbon oriented trans to the axially bound pyridine. A similar trend is observed in the [($\mathbf{L^{0\rightarrow 2}}$)$_2$Cu]$^+$ Cu(I) structures; the most bulky pyridine subunit is always positioned in the least sterically demanding position. In [($\mathbf{L^{0\rightarrow 2}}$)$_2$Cu]$^{2+}$, the methoxypyridines are preferentially positioned into the axial positions. While no preference exists in [($\mathbf{L^0}$)$_2$Cu]$^{2+}$, only one configuration is possible in [($\mathbf{L^1}$)$_2$Cu]$^{2+}$; both methoxypyridine subunits reside in the axial positions. A noticeable distortion in this complex is the off-axis positioning of the axial methoxypyridines and the skewing of the equatorial pyridines such that the Cu(II)−N(py) bond distances are markedly different (2.006 vs 2.072 Å). The equatorial Cu−N distances in [($\mathbf{L^0}$)$_2$Cu]$^{2+}$ are more uniform even though all the equatorial ligands are 6-H-pyridines in both structures. A similar distortion in the structure of [(tris(1-pyrazoyl)borate)$_2$Cu]$^{2+}$ is thought to rise from dynamic fluxional behavior in this Jahn−Teller system.[45] In [($\mathbf{L^2}$)$_2$Cu]$^{2+}$, one methoxypyridine binds axially, while the remaining methoxypyridine must bind in an equatorial position. This methoxypyridine is disordered over the two equatorial positions, which results in a slight decrease in the equatorial Cu(II)−N(py) bond distances, as compared to [($\mathbf{L^0}$)$_2$Cu]$^{2+}$ and [($\mathbf{L^1}$)$_2$Cu]$^{2+}$. This unexpected result is primarily due to a simplified treatment of the methoxypyridine occupancies in the structural determination.

Two crystal structures of the most sterically demanding ligand, $\mathbf{L^3}$, with Cu(II) show coordination distortions to accommodate all three methoxypyridine ligands. When crystallized anaerobically, a bis-ligated complex [($\mathbf{L^3}$)$_2$Cu]$^{2+}$ is isolated. The structure differs from the [($\mathbf{L^{0\rightarrow 2}}$)$_2$Cu]$^{2+}$ complexes, with one ligand inverted such that the bridgehead methoxy oxygen atom

---

(45) The tetragonality ($T$) of these complexes are the following: [($\mathbf{L^0}$)$_2$Cu]$^{2+}$, 0.85; [($\mathbf{L^1}$)$_2$Cu]$^{2+}$, 0.87; [($\mathbf{L^2}$)$_2$Cu]$^{2+}$, 0.82; [($\mathbf{L^3}$)$_2$Cu]$^{2+}$, 0.89 where $T$ = (mean in-plane Cu−L bond distance/mean out-of-plane Cu−L bond distance). Generally, most Cu(II) tetragonally distorted complexes with $T$ values in the range of 0.80−0.85 have static structures, while complexes with $T$ values >0.85 suggest potential dynamic distortions; see: Murphy, A.; Hathaway, B. J.; King, T. J. *J. Chem. Soc., Dalton Trans.* **1979**, *11*, 1646−1650.

**Table 5.** Selected Bond Distances (Å) and Angles (deg) for the Cupric Complexes

| $[(\mathbf{L}^0)_2\mathrm{Cu}](\mathrm{OTf})_2$ | | $[(\mathbf{L}^1)_2\mathrm{Cu}](\mathrm{OTf})_2\cdot(\mathrm{CH_3CN})$ | | $[(\mathbf{L}^2)_2\mathrm{Cu}](\mathrm{OTf})_2$ | |
|---|---|---|---|---|---|
| Cu1···N1 | 2.365(2) | Cu1···N1 | 2.343(2) | Cu1···N1 | 2.467(6) |
| Cu1−N2 | 1.997(2) | Cu1−N2 | 2.001(2) | Cu1−N2 | 2.026(6) |
| Cu1−N3 | 2.033(2) | Cu1−N3 | 2.077(2) | Cu1−N3 | 2.007(6) |
| N1−Cu1−N2 | 84.2(1) | N1−Cu1−N2 | 83.47(9) | N1−Cu1−N2 | 96.5(2) |
| N1−Cu1−N3 | 86.0(1) | N1−Cu1−N3 | 86.91(9) | N1−Cu1−N3 | 85.5(2) |
| N2−Cu1−N3 | 86.1(1) | N2−Cu1−N3 | 86.82(9) | N2−Cu1−N3 | 85.6(2) |

| $[(\mathbf{L}^3)_2\mathrm{Cu}](\mathrm{OTf})\cdot(\mathrm{acetone})$ | | $[\mathbf{L}^3\mathrm{Cu}(\mathrm{H_2O})_3](\mathrm{OTf})\cdot(\mathrm{H_2O})$ | |
|---|---|---|---|
| Cu1···N1 | 2.352(4) | Cu1−N2 | 2.030(3) |
| Cu1−N2 | 2.060(4) | Cu1−N3 | 2.040(3) |
| Cu1−N3 | 2.034(4) | Cu1···O1 | 2.374(3) |
| Cu1···O5 | 2.275(3) | Cu1−O5 | 1.994(3) |
| Cu1−N5 | 2.108(4) | Cu1−O6 | 1.979(3) |
| Cu1−N6 | 2.073(4) | Cu1···O13 | 2.321(3) |
| N1−Cu1−N2 | 88.0(2) | N2−Cu1−N3 | 84.6(1) |
| N1−Cu1−N3 | 85.9(2) | N2−Cu1−O1 | 74.1(1) |
| N2−Cu1−N3 | 86.1(2) | N2−Cu1−O5 | 95.3(1) |
| O5−Cu1−N5 | 74.5(1) | N2−Cu1−O6 | 165.0(1) |
| O5−Cu1−N6 | 72.0(1) | N2−Cu1−O13 | 109.3(1) |
| N5−Cu1−N6 | 85.8(2) | N3−Cu1−O1 | 74.9(1) |
| N1−Cu1−O5 | 163.6(2) | N3−Cu1−O5 | 167.6(1) |
| N2−Cu1−N5 | 176.4(2) | N3−Cu1−O6 | 91.1(1) |
| N3−Cu1−N6 | 179.4(2) | N3−Cu1−O13 | 109.1(1) |

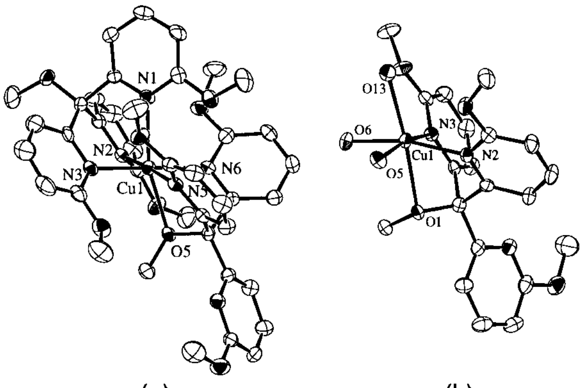

(a) (b)

**Figure 5.** ORTEP representations (50% probability) without hydrogens for the cupric complexes (a) $[(\mathbf{L}^3)_2\mathrm{Cu}]^{2+}$ and (b) $[\mathbf{L}^3\mathrm{Cu}(\mathrm{H_2O})_3]^{2+}$.

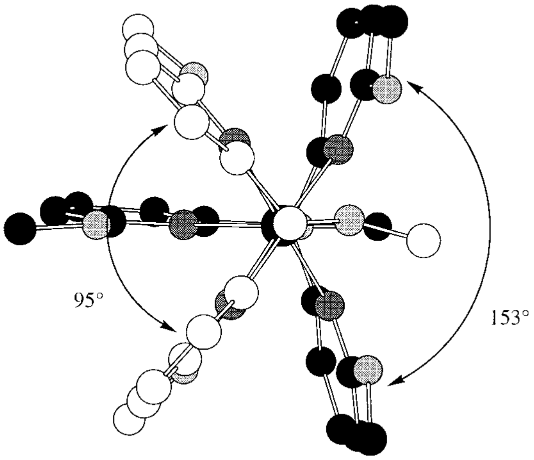

**Figure 6.** View down the axial coordination axis of the $[(\mathbf{L}^3)_2\mathrm{Cu}]^{2+}$ complex (excluding the nonligated methoxypyridine subunit) with the lower ligand carbon atoms as black spheres and the upper ligand carbon atoms as white spheres.

and two methoxypyridines bind in a facial-capping *N,N′,O* coordination. The bridgehead ether oxygen acts as the weak axial donor, while the two methoxypyridines are equatorially positioned. The remaining methoxypyridine is rotated away from the copper center (Figure 5a). This inversion of the one ligand and use of the ether functional group significantly reduces the steric congestion in the vicinity of the copper. The angle between the two equatorially bound pyridines of the inverted ligand is dramatically decreased as compared to the angle in the conventionally bound ligand (95 vs 153°; Figure 6). For the complex to adopt an inversion symmetric *N,N′,N″* "bis-tris" configuration would require all four equatorial bound pyridines to be positioned in close proximity, necessitating a considerable lengthening of the Cu(II)−N(py) bonds. The *N,N′,O* ligand configuration allows for reasonably short equatorial Cu(II)−N(py) bond distances (Table 5) while maintaining reasonable axial stabilization (Cu1−O1 = 2.275(3) Å).

Even the coordination environment of $[(\mathbf{L}^3)_2\mathrm{Cu}]^{2+}$ is strained as evidenced by its conversion to a $[\mathbf{L}^3\mathrm{Cu}(\mathrm{H_2O})_3]^{2+}$ complex with release of the second equivalent of $\mathbf{L}^3$ upon expose to air (Figure 5b). In $[\mathbf{L}^3\mathrm{Cu}(\mathrm{H_2O})_3]^{2+}$ the ligand is again inverted to provide a facial-capping *N,N′,O* coordination. This allows close coordination of both the pyridine ligands in the equatorial plane and the two equatorial bound water molecules. Comparison of metrical parameters for both the Cu(II) complexes of $\mathbf{L}^3$ (Table 5) shows that the equatorial bond lengths can be significantly shortened by exchange of the sterically demanding ligand with water molecules.

**Solution Structures.** The greater spatial demands of the methoxypyridine groups are evident not only in the solid state, but also in the solution behavior. The two different coordination modes found in the solid state for the Cu(I) complexes, $[\mathbf{L}\mathrm{Cu}(\mathrm{CH_3CN})]^+$ and $[(\mathbf{L})_2\mathrm{Cu}]^+$, are fully consistent with their solution behavior. The species distribution between these two cuprous forms is controlled by stoichiometry. For Cu(II), the spectroscopic trends observed by varying the ligands are consistent with the degree of tetragonal distorted observed in the solid state.

Reactions of equimolar amounts of $\mathbf{L}^{0-2}$ with $[\mathrm{Cu^I}(\mathrm{CH_3CN})_4](\mathrm{OTf})$ in acetone or $\mathrm{CH_2Cl_2}$ result in pale yellow solutions of the three Cu(I) complexes. The UV/vis spectra are indistinguishable with only a single significant peak near $\lambda = 338$ nm. The energy and intensity of these transitions are consistent with metal to ligand charge-transfer transitions (MLCT) as the free ligand absorbs at $\lambda < 310$ nm. Comparison of the $^1$H NMR spectra of the appropriate free ligand with the 1:1 Cu:$\mathbf{L}^{0-3}$

**Table 6.** $^1$H NMR Shifts of Bridgehead Methoxy and 6-H Pyridine Protons for Cu(I) Complexes[a]

| | free ligand | | [**L**Cu(CH$_3$CN)]$^+$ | | [**L**Cu(CO)]$^+$ | | [**L**Cu(PPh$_3$)]$^+$ | | [(**L**)$_2$Cu]$^+$ | |
|---|---|---|---|---|---|---|---|---|---|---|
| ligand | OMe | 6-H | OMe | 6-H | OMe | 6-H | OMe | 6-H | OMe | 6-H |
| **L$^0$** | 3.29 | 8.62 | 3.78 | 8.71 | 4.02 | 9.01 | 4.00 | 8.31 | 3.12 | 7.46 |
| **L$^1$** | 3.32 | 8.59 | 3.44 | 8.66 | 3.97 | 8.99 | 3.90 | 8.29 | 3.16 | 7.50 |
| **L$^2$** | 3.33 | 8.59 | 3.36 | 8.65 | 3.95 | 8.97 | 3.73 | 8.25 | 3.15 | 7.46 |
| **L$^3$** | 3.40 | − | 3.31 | − | 3.93 | − | 3.48 | − | | |

[a] Shifts are reported in ppm from a TMS internal reference.

products ([**L$^{0\to3}$**Cu(CH$_3$CN)]$^+$) show that the bridgehead methoxy group is a sensitive probe to metal binding, generally shifting downfield upon metal complexation. The ability of these remotely positioned protons to signal metal binding is readily understood from the solid-state structures, which show that the bridgehead methoxy group plays an important structural role when the ligands adopt a facial-capping *N,N′,N″* configuration (*vide supra*). When the ratio of ligand to Cu(I) increases from 1:1 to 2:1, both the UV/vis and $^1$H NMR features change. The symmetry of the $^1$H NMR spectra is consistent with [(**L$^{0\to2}$**)$_2$Cu]$^+$ complexes with equivalent ligands. The nearly identical UV/vis spectra, with a single MLCT band near $\lambda$ = 436 nm, is also consistent with a set of isostructural complexes for [(**L$^{0\to2}$**)$_2$Cu]$^+$. At ligand-to-metal ratios above 2:1, the spectroscopic features do not change. Adjustment of the ratio back to 1:1 by addition of [Cu$^I$(CH$_3$CN)$_4$](OTf) gives back the spectra of the monoligated Cu(I) complexes, indicating that the system is in rapid equilibrium (eq 4).

$$[\mathbf{L}^{0\to2}\mathrm{Cu^I(CH_3CN)](OTf)} \xrightleftharpoons[\mathrm{[Cu^I(CH_3CN)_4](OTf)}]{\mathbf{L}^{0\to2}} [(\mathbf{L}^{0\to2})_2\mathrm{Cu^I](OTf)} \quad (4)$$

Reaction of an equimolar amount of **L$^3$** with [Cu$^I$(CH$_3$CN)$_4$](OTf) in acetone or CH$_2$Cl$_2$ results in a pale yellow solution of the Cu(I) complex. UV/vis and $^1$H NMR spectra are consistent with a single species, and increasing the ratio of ligand to metal does not change the UV/vis spectra in the 350−500 nm range or the NMR spectra of the metal complex. The increased steric demands of **L$^3$** apparently preclude the formation of any type of [(**L$^3$**)$_2$Cu]$^+$ complex both in solution and solid state.

The symmetry of the $^1$H NMR spectra for the 1:1 reactions of **L$^{0\to3}$** and [Cu$^I$(CH$_3$CN)$_4$]$^+$ are consistent with the formation of a distorted tetrahedral Cu(I) complex with an axial CH$_3$CN ligand, [**L$^{0\to3}$**Cu(CH$_3$CN)]$^+$. A single peak for bound and unbound CH$_3$CN indicates rapid CH$_3$CN exchange on the NMR time scale. The [**L$^{0\to2}$**Cu(CH$_3$CN)]$^+$ complexes rapidly convert to [(**L**)$_2$Cu]$^+$ upon addition of 1 equiv of ligand as assessed by $^1$H NMR. Associated with this conversion is a noticeable upfield shift of the 6-H pyridine resonance of the ligated nonmethoxypyridines from ~8.65 ppm in [**L$^{0\to2}$**Cu(CH$_3$CN)]$^+$ to nearly ~7.5 in [(**L$^{0\to2}$**)$_2$Cu]$^+$ (Table 6). Since the 6-H chemical shifts of [**L$^{0\to2}$**Cu(CH$_3$CN)]$^+$ are similar to their free ligand, the significant upfield shift of the 6-H proton peak in [(**L$^{0\to2}$**)$_2$Cu]$^+$ is consistent with their positioning above the ligating pyridine rings of the second ligand of the complex as clearly indicated in the solid-state structures.

While the three [(**L$^{0\to2}$**)$_2$Cu]$^+$ complexes are stable under aerobic conditions, each exhibits variable intra- and inter-ligand lability. All the pyridine subunits in [(**L$^0$**)$_2$Cu]$^+$ are equivalent by $^1$H NMR as are the methoxypyridine subunits in [(**L$^2$**)$_2$Cu]$^+$. This equivalence contrasts with the crystal structures which show distinctly ligated and unligated pyridine subunits. A facile subunit exchange within any one ligand from an unligated to ligated position must occur faster than the NMR time scale. This pyridine subunit exchange likely proceeds through one of two dissociative mechanisms, distinguished by the coordination number of the intermediate species.

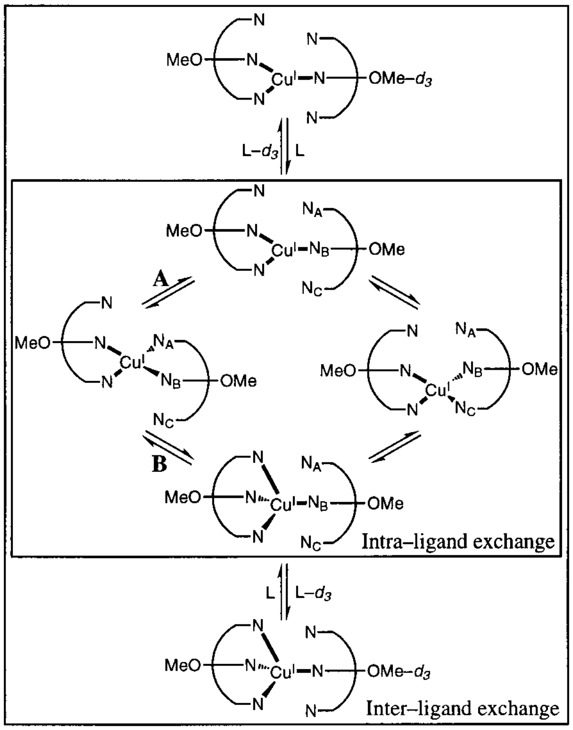

**Figure 7.** Intra-ligand exchange proceeds through either a dissociation (**A**) or rearrangement (**B**) rate-determining mechanistic step. Possible inter-ligand exchange likely proceeds through a monodentate intermediate (**L**-*d*$_3$ is a deuterated analog of **L**). The results of intra- and inter-ligand exchange experiments are most consistent with pathway **B**.

One possible mechanism (**A**) involves a 3-coordinate, trigonal planar intermediate generated by dissociation of a single pyridine subunit, followed by reorganization of the three ligating pyridines into a trigonal planar coordination (Figure 7). Such trigonal planar coordination is commonly found for Cu(I) complexes, especially those in biological systems. Pivoting of the monoligated ligand, followed by rebinding allows facile intra-ligand subunit conversion. A second possible mechanism (**B**) involves a 4-coordinate, pseudo-tetrahedral intermediate. In this mechanism, one of the unbound pyridine subunits within [(**L**)$_2$Cu]$^+$ displaces a bound pyridine of the second ligand envisioned to occur through a 5-coordinate, trigonal bipyramidal transition state. The resulting 4-coordinate intermediate has one facial-capping ligand (*N,N′,N″* coordination) and the other ligand bound in a monodentate fashion. Monodentate ligation allows facile ligand pivoting and rebinding with displacement of one of the three subunits of the facial capping ligand. This leads to intra-ligand subunit conversion. The intermediate in the latter mechanism is structurally similar to the structurally characterized [**L**Cu(CH$_3$CN)]$^+$ form, except that the CH$_3$CN is displaced by a pyridine ligand. If either mechanism of intra-ligand exchange is operative, inter-ligand exchange would likely proceed through

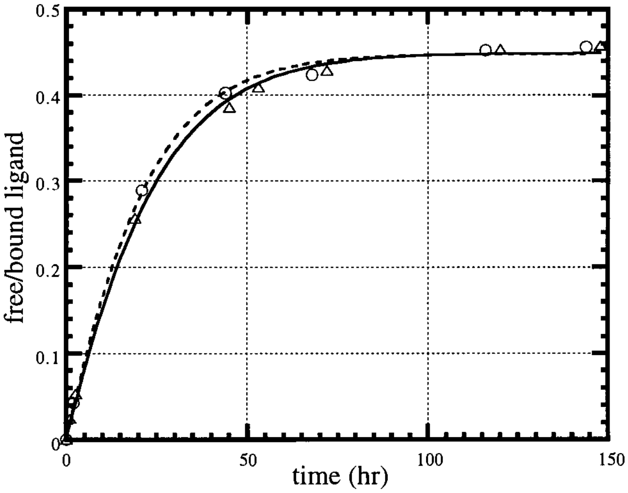

**Figure 8.** Plot of the $^1$H NMR monitored intra-ligand exchange in acetone-$d_6$ at RT of the addition of 1 equiv of $\mathbf{L^1}$ into $[(\mathbf{L^1}\text{-}d_3)_2\mathrm{Cu}]^+$ (△) and 1 equiv of $\mathbf{L^1}$-$d_3$ into $[(\mathbf{L^1})_2\mathrm{Cu}]^+$ (○).

the monodentate intermediate form. Indeed, if excess ligand is added to solutions of $[(\mathbf{L^0})_2\mathrm{Cu}]^+$ and $[(\mathbf{L^2})_2\mathrm{Cu}]^+$ complexes, the resonances of the free ligand and metal complexes coalesce, consistent with facile inter-ligand exchange on the NMR time scale.

The intra- and inter-ligand exchange behavior of $[(\mathbf{L^1})_2\mathrm{Cu}]^+$ contrasts dramatically with that of other two $[(\mathbf{L})_2\mathrm{Cu}]^+$ complexes ($\mathbf{L} = \mathbf{L^0}, \mathbf{L^2}$), even though their structural attributes appear similar. The symmetry of the $^1$H NMR spectrum of $[(\mathbf{L^1})_2\mathrm{Cu}]^+$ shows that the two nonmethoxypyridines are equivalently ligated to Cu(I), and that the 6-H protons are significantly shielded relative to the free ligand (Table 6). Both results suggest a $[(\mathbf{L^1})_2\mathrm{Cu}]^+$ structure similar to $[(\mathbf{L^0})_2\mathrm{Cu}]^+$ or $[(\mathbf{L^2})_2\mathrm{Cu}]^+$. The $^1$H NMR spectrum differs in that the 3-H protons of the methoxypyridine are significantly shielded (6.4 ppm), which is consistent with the nonligated subunit residing in the shielding region of another pyridine ring. This indicates slowed intra-ligand rotation in $[(\mathbf{L^1})_2\mathrm{Cu}]^+$ relative to $[(\mathbf{L^0})_2\mathrm{Cu}]^+$ and $[(\mathbf{L^2})_2\mathrm{Cu}]^+$. This slowed intra-ligand exchange behavior logically leads to slowed inter-ligand exchange; free $\mathbf{L^1}$ and $[(\mathbf{L^1})_2\mathrm{Cu}]^+$ do not exchange ligands on the NMR time scale as indicated by two independent sets of $^1$H NMR resonances. The *intra-ligand* rotation is presumably important in facilitating *inter-ligand* exchange in $[(\mathbf{L})_2\mathrm{Cu}]^+$ species.

A more direct examination of the inter-ligand exchange process of the $[(\mathbf{L^{0\to 2}})_2\mathrm{Cu}]^+$ complexes is possible through competitive binding experiments with ligands deuterated in the bridgehead methoxy group. The ligand exchange process is readily followed by integration of the bridgehead methoxy group of the free and bound ligand when either free deutero-ligand ($(\mathbf{L^{0\to 2}}\text{-}d_3)$ is added to the proto-ligand metal complexes, $[(\mathbf{L^{0\to 2}}\text{-}h_3)_2\mathrm{Cu}]^+$ or vice versa. When this experiment is performed with either $\mathbf{L^0}$-$d_3$ or $\mathbf{L^2}$-$d_3$ and $[(\mathbf{L^0}\text{-}h_3)_2\mathrm{Cu}]^+$ or $[(\mathbf{L^2}\text{-}h_3)_2\mathrm{Cu}]^+$, respectively, equilibrium is reached in less than the mixing and acquisition time at RT ($<10^2$ s). In contrast, equilibration of $\mathbf{L^1}$-$d_3$ with $[(\mathbf{L^1}\text{-}h_3)_2\mathrm{Cu}]^+$ requires over 100 h ($3.6 \times 10^5$ s) at RT (Figure 8), an inter-ligand exchange rate $10^3-10^4$ times slower than the rate for either $[(\mathbf{L^0})_2\mathrm{Cu}]^+$ or $[(\mathbf{L^2})_2\mathrm{Cu}]^+$. The ostensibly innocent substitution of one methoxypyridine into $\mathbf{L^0}$ to generate $\mathbf{L^1}$ dramatically effects ligand lability. Further substitution of $\mathbf{L^1}$ by an additional methoxypyridine in $\mathbf{L^2}$ returns the inter- and intra-ligand lability.

The large differences in intra- and inter-ligand exchange among these $[(\mathbf{L^{0\to 2}})_2\mathrm{Cu}]^+$ complexes, the lack of formation of a $[(\mathbf{L^3})_2\mathrm{Cu}]^+$ complex, and the ligation preference of the nonmethoxypyridine subunits in these complexes combine to support dissociative mechanism **B**. If the 3-coordinate intermediate mechanism, **A**, were operative, inter-ligand dissociation rates of $[(\mathbf{L^0})_2\mathrm{Cu}]^+$ and $[(\mathbf{L^1})_2\mathrm{Cu}]^+$ should be comparable, as both ligands provide identical pyridine coordination for the Cu(I), and the rate-determining step in this process is presumably the initial dissociation of bound ligand. Further support of mechanism **B** is that it logically relates inter- to intra-ligand exchange, a phenomena not readily explained by **A**. In all cases of fast intra-ligand exchange ($[(\mathbf{L^0})_2\mathrm{Cu}]^+$ and $[(\mathbf{L^2})_2\mathrm{Cu}]^+$), the unligated pyridine always can displace a ligated pyridine of comparable type (unligated pyridine for ligated pyridine in $[(\mathbf{L^0})_2\mathrm{Cu}]^+$; unligated methoxypyridine for ligated methoxypyridine in $[(\mathbf{L^2})_2\mathrm{Cu}]^+$). In contrast, an energetically unfavorable displacement of a ligated nonmethoxypyridine by an unligated methoxypyridine is necessary with $[(\mathbf{L^1})_2\mathrm{Cu}]^+$ to generate the intermediate necessary for both facile intra- and inter-ligand exchange. It is this less energetically favorable process which is possibly responsible for the slowed intra-ligand exchange which in turn reduces the potential for inter-ligand exchange through the 4-coordinate intermediate.

Further insights into the destabilizing effects of methoxypyridines on Cu(I) complexes can be assessed through mixed ligand competitive binding experiments on the $[(\mathbf{L^{0\to 2}})_2\mathrm{Cu}]^+$ complexes followed by $^1$H NMR in acetone.[46] Competition studies between different $[(\mathbf{L})_2\mathrm{Cu}]^+$ species ($\mathbf{L} = \mathbf{L^{0\to 2}}$) indicate that $[(\mathbf{L^2})_2\mathrm{Cu}]^+$ is the least stable of the three complexes, and that $[(\mathbf{L^1})_2\mathrm{Cu}]^+$ and $[(\mathbf{L^0})_2\mathrm{Cu}]^+$ have comparable stability. $\mathbf{L^0}$ or $\mathbf{L^1}$ quickly replace both ligands of $[(\mathbf{L^2})_2\mathrm{Cu}]^+$, while neither $\mathbf{L^2}$ nor $\mathbf{L^3}$ is able to displace the ligands in $[(\mathbf{L^0})_2\mathrm{Cu}]^+$ and $[(\mathbf{L^1})_2\mathrm{Cu}]^+$. The competitive experiment with $\mathbf{L^0}$ and $\mathbf{L^1}$ attains an equilibrium statistical mixture of all three possible products, $[(\mathbf{L^0})_2\mathrm{Cu}]^+$, $[(\mathbf{L^1})_2\mathrm{Cu}]^+$, and $[\mathbf{L^0}\mathbf{L^1}\mathrm{Cu}]^+$, after ~100 h at RT. As both ligands bind Cu(I) with two nonmethoxypyridines, the lack of preference for one ligand over the other in this bis-ligated species is not surprising. The slow equilibration is also in line with the slow exchange rate of $\mathbf{L^1}$ which dominates the overall exchange rate of the mixed system.

Reactions of two equivalents of $\mathbf{L^{0\to 3}}$ with $\mathrm{Cu^{II}(OTf)_2}$ in acetone or $CH_2Cl_2$ result in the formation of complexes with the general formula $[(\mathbf{L^{0\to 3}})_2\mathrm{Cu}](\mathrm{OTf})_2$. UV/Vis titrations do not indicate the presence of any intermediate species in the formation of $[(\mathbf{L^{0\to 3}})_2\mathrm{Cu}]^{2+}$. Excess ligand is observed in the $^1$H NMR spectra of the reactions when the ratio of ligand to metal is increased above 2:1, suggesting either a lack of or slow inter-ligand exchange in all the $[(\mathbf{L^{0\to 3}})_2\mathrm{Cu}]^{2+}$ complexes.

A $d^9$ Cu(II) ion ligated by six equivalent ligands is predicted to undergo Jahn–Teller distortion. Generally, this tetragonal distortion involves an axial elongation that results in a square-planar complex in the distortion limit. The magnitude of this distortion is primarily determined by the ligand field strength; however, the flexibility and steric demands of the ligands also are determinants.[47,48] As the methoxy- and nonmethoxypyridines are expected to have similar ligand field strengths, the extent of tetragonal distortion in $[(\mathbf{L^{0\to 3}})_2\mathrm{Cu}]^{2+}$ should correlate with the ligand steric bulk; with less bulk, shorter Cu–N(py) bonds can be realized in the equatorial plane, leading to a greater axial distortion. This distortion should be manifest in the energy

---

(46) Assessing the relative stability of the $[\mathbf{L^{0\to 2}}\mathrm{Cu}(\mathrm{CH_3CN})]^+$ complexes is complicated by the formation of the bis-ligated species upon addition of free ligand.

(47) Solomon, E. I. *Comments Inorg. Chem.* **1984**, *3*, 227–320.

(48) Hathaway, B. J. *Struct. Bonding (Berlin)* **1984**, *57*, 55–118.

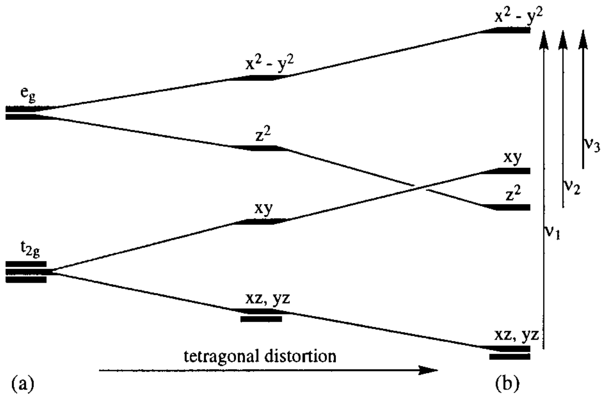

**Figure 9.** Diagram of the d-orbital ligand field energy tetragonal distortion from (a) an octahedral to (b) a square-planar geometry.

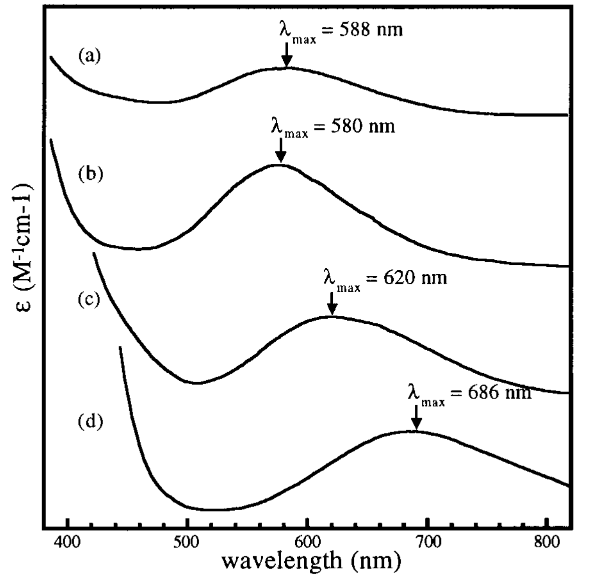

**Figure 10.** UV/vis spectra in $CH_2Cl_2$ for (a) $[(\mathbf{L^0})_2Cu]^{2+}$, (b) $[(\mathbf{L^1})_2Cu]^{2+}$, (c) $[(\mathbf{L^2})_2Cu]^{2+}$, and (d) $[(\mathbf{L^3})_2Cu]^{2+}$.

of the d−d electronic transitions in Cu(II); as the distortion approaches the square-planar limit, the d−d electronic transitions should increase in energy (Figure 9). Additionally, the $g_{||}$ values EPR parameters of the Cu(II) center should also reflect the relative distortion in the electronic ground state as this value is inversely related to the difference in energy of the $d_{x^2-y^2}$ and the $d_{xy}$ orbitals in an axially distorted system.[47]

The EPR and optical parameters of $[(\mathbf{L^2})_2Cu]^{2+}$ and $[(\mathbf{L^3})_2Cu]^{2+}$ significantly vary relative to $[(\mathbf{L^0})_2Cu]^{2+}$ and $[(\mathbf{L^1})_2Cu]^{2+}$, suggesting differing degrees of a tetragonal distortion. The energy of the Cu(II) d−d transitions in the visible range (Figure 10) increases with reduction of the bulk of the ligands. The energy of the transitions for $[(\mathbf{L^0})_2Cu]^{2+}$ and $[(\mathbf{L^1})_2Cu]^{2+}$ are similar, but occur at a higher energy than either of the transitions of $[(\mathbf{L^2})_2Cu]^{2+}$ and $[(\mathbf{L^3})_2Cu]^{2+}$. This trend is fully consistent with the solid-state structural parameters which suggest that $[(\mathbf{L^0})_2Cu]^{2+}$ and $[(\mathbf{L^1})_2Cu]^{2+}$ have a more "square-planar" geometry. The spectral similarities for $[(\mathbf{L^0})_2Cu]^{2+}$ and $[(\mathbf{L^1})_2Cu]^{2+}$ are not surprising given that both have only nonmethoxypyridine ligands in their equatorial planes. The decrease in the $g_{||}$ EPR values from $[(\mathbf{L^3})_2Cu]^{2+}$ through $[(\mathbf{L^0})_2Cu]^{2+}$ is again consistent with the least sterically bulky complexes attaining a more square-planar geometry (Figure 11). Thus, all solution spectroscopic data are fully consistent with the structural trends observed in the solid state.

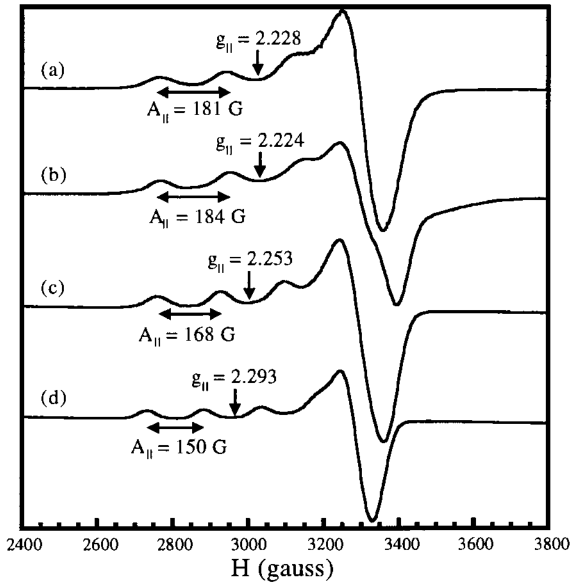

**Figure 11.** EPR spectra for at 77 K in $CH_2Cl_2$ (a) $[(\mathbf{L^0})_2Cu]^{2+}$, (b) $[(\mathbf{L^1})_2Cu]^{2+}$, (c) $[(\mathbf{L^2})_2Cu]^{2+}$, and (d) $[(\mathbf{L^3})_2Cu]^{2+}$.

**Scheme 3**

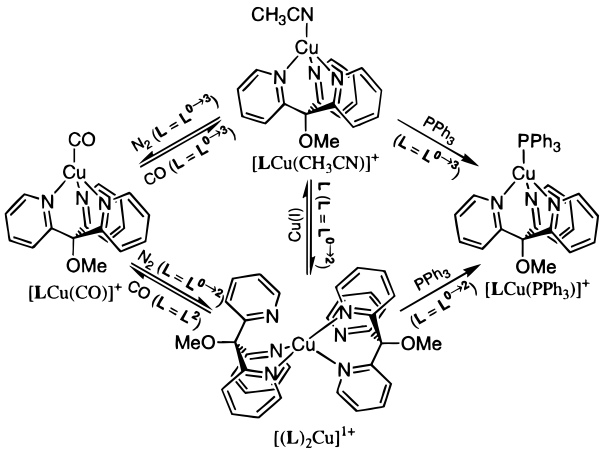

**Ligand Substitution of Cu(I) Complexes.** The $[\mathbf{L}Cu(CH_3CN)]^+$ complexes ($\mathbf{L} = \mathbf{L^{0\rightarrow3}}$) are stable under anaerobic conditions, while exposure to air results in slow oxidation to various Cu(II) species. However, all three $[(\mathbf{L^{0\rightarrow2}})_2Cu]^+$ complexes are indefinitely stable even under aerobic conditions. The reaction of the seven Cu(I) complexes with excess CO(g) again highlights the instability introduced by inclusion of the methoxypyridine subunits in the ligands (Scheme 3). When acetone or $CH_2Cl_2$ solutions of $[\mathbf{L^{0\rightarrow3}}Cu(CH_3CN)]^+$ are flushed with 1 atm of CO(g), the yellow solutions visibly bleach forming $[\mathbf{L^{0\rightarrow3}}Cu(CO)]^+$ as assessed by $^1H$ NMR. Curiously, the 6-H resonance of $[\mathbf{L^{0\rightarrow2}}Cu(CO)]^+$ show significantly larger downfield shifts from the free ligand as compared to the $CH_3CN$ adducts (Table 6). A similar deshielding is seen in the bridgehead methoxy protons. The CO stretching bands near 2100 $cm^{-1}$ for each complex do not significantly vary for $[\mathbf{L^{0\rightarrow3}}Cu(CO)]^+$ (($cm^{-1}$) $\mathbf{L^0}$ (2102); $\mathbf{L^1}$ (2100); $\mathbf{L^2}$ (2096); $\mathbf{L^3}$ (2093)). As CO stretching frequencies generally correlate with the electronic properties of a metal center, the small changes observed are consistent with only slightly greater electronic donation by a methoxypyridine as compared to the 6-H-pyridine ligands when steric interactions of the 6-substituents do not dictate distortions in the coordination sphere. Much greater

**Table 7.** Electrochemical Data for Cu(I) and Cu(II) Complexes[a]

| complex | solvent | $E_{ox}$ (mV) | $E_{red}$ (mV) | $E_{1/2}$ (mV) | $\Delta E$ (mV) |
|---|---|---|---|---|---|
| $[\mathbf{L^0}Cu(CH_3CN)]^+$ | 20% $CH_3CN/CH_2Cl_2$ | 575 | 440 | 510 | 135 |
| $[\mathbf{L^1}Cu(CH_3CN)]^+$ | 20% $CH_3CN/CH_2Cl_2$ | 680 | 490 | 585 | 170 |
| $[\mathbf{L^2}Cu(CH_3CN)]^+$ | 20% $CH_3CN/CH_2Cl_2$ | 710 | 600 | 655 | 110 |
| $[\mathbf{L^3}Cu(CH_3CN)]^+$ | 20% $CH_3CN/CH_2Cl_2$ | 870 | 600 | 735 | 270 |
| $[(\mathbf{L^0})_2Cu]^+$ | $CH_2Cl_2$ | 490 | −70 | | |
| $[(\mathbf{L^1})_2Cu]^+$ | $CH_2Cl_2$ | 460 | −10 | | |
| $[(\mathbf{L^2})_2Cu]^+$ | $CH_2Cl_2$ | 390 | −40 | | |
| $[(\mathbf{L^0})_2Cu]^{2+}$ | $CH_2Cl_2$ | −50 | 500 | | |
| $[(\mathbf{L^1})_2Cu]^{2+}$ | $CH_2Cl_2$ | −20 | 460 | | |
| $[(\mathbf{L^2})_2Cu]^{2+}$ | $CH_2Cl_2$ | −50 | 430 | | |

[a] The $Fc/Fc^+$ couple was used as an internal reference, with $E_{1/2}$ = 450 mV (vs SCE).

changes in CO stretching frequency have been observed in other systematic studies of facial-capping trinitrogen ligands with Cu(I).[13,49]

While the $[\mathbf{L^{0\to3}}Cu(CH_3CN)]^+$ complexes react in a consistent manner with CO, a difference is observed in the reactivity of CO with the $[(\mathbf{L^{0\to2}})_2Cu]^+$ complexes. $[(\mathbf{L^0})_2Cu]^+$ and $[(\mathbf{L^1})_2Cu]^+$ are stable to 1 atm of CO(g), while $[(\mathbf{L^2})_2Cu]^+$ is cleanly and rapidly converted to $[\mathbf{L^2}Cu(CO)]^+$ and an equivalent of the free ligand ($^1$H NMR). In contrast, triphenylphosphine cleanly reacts with all seven Cu(I) complexes to form the $[\mathbf{L^{0\to3}}Cu(PPh_3)]^+$ complexes (Scheme 3). These monophosphine complexes are rather robust, as large excesses of free ligand, CO, or $CH_3CN$ do not alter their composition.

**Electrochemistry.** Cyclic voltammetry (CV) performed on solutions of $[\mathbf{L^{0\to3}}Cu(CH_3CN)]^+$ in $CH_2Cl_2$ reveals irreversible oxidations at moderately positive potentials. Similar irreversible electrochemical behavior is found in a series of $[Tp^{RR'}Cu(CH_3CN)]^+$ complexes ($Tp^{RR'}$ = tris(3-*R*,5-*R'*-pyrazoyl)hydroborate).[50] The CV oxidative behavior of $[\mathbf{L^{0\to3}}Cu(CH_3CN)]^+$ is significantly improved if $CH_3CN$ is included (ca. 20% v/v; Table 7); the oxidation process likely involves the binding of an additional $CH_3CN$ ligand to generate a more stable 5-coordinate Cu(II) complex. An increased CV oxidation potential correlates with greater steric hindrance of the ligands. If addition ligation is required in this process, the driving force needed to oxidize the metal should increase as observed. The largest difference in potential occurs between $[\mathbf{L^2}Cu(CH_3CN)]^+$ and $[\mathbf{L^3}Cu(CH_3CN)]^+$ (Table 7) which suggests that $\mathbf{L^3}$, bound in a facial-capping *N*,*N'*,*N''* conformation, only reluctantly accommodates a fifth ligand; this behavior nicely coincides with the structure of $[\mathbf{L^3}Cu(H_2O)_3]^{2+}$ which has $\mathbf{L^3}$ inverted to allow a closer approach by the two equatorially ligated water molecules.

The difference in the preferred ligation geometry of Cu(I) and Cu(II) is also likely responsible for the irreversible CV oxidation behavior of $[(\mathbf{L^{0\to2}})_2Cu]^+$ and irreversible CV reduction behavior of $[(\mathbf{L^{0\to2}})_2Cu]^{2+}$. The close correlation of the oxidation and reduction potentials for the cuprous and cupric species of a single ligand, respectively, suggests that the redox process is associated with a ligand rearrangement (Table 7). Though CV suggests an irreversible process, cycling of the oxidation and reduction does not show significant decrease in the signal, consistent with a slow ligand rearrangement to accommodate the preferred coordination geometry of each oxidation state of copper.

## Summary

An efficient modular synthesis of sterically hindered tris(2-pyridyl)methoxymethane ligands is presented which allows for various functional groups to be positioned at the periphery of the metal binding cavity. Appropriate substitution of the pyridine subunits is found to dramatically increase the synthetic yields of the reactions used to assemble these ligands. The ligand syntheses and copper chemistry of a simple series of these ligands with methoxy substituents are presented as an initial systematic study of this class of ligand. Varying the number of methoxy groups at the periphery produces only subtle changes in copper coordination geometry and ligand exchange behavior. However, in the extreme case of three methoxypyridine subunits, the copper coordination chemistry changes dramatically. These observations are consistent with the enhanced spatial demands of the trisubstituted ligands precluding the preferred ligation observed in the simpler ligands.

Throughout this study, the solution structures of the copper complexes closely correlate with the solid-state data for both the Cu(I) and Cu(II) complexes. Two different types of distorted tetrahedral $N_4$-cuprous complexes are formed depending on the ligand to metal stoichiometry: $[\mathbf{L^{0\to3}}Cu(CH_3CN)]^+$ and $[(\mathbf{L^{0\to2}})_2Cu]^+$. A tetrahedrally ligated Cu(I) with four methoxypyridines is not observed as $\mathbf{L^3}$ only forms $[\mathbf{L^3}Cu(CH_3CN)]^+$, even with greater than 2 equiv of $\mathbf{L^3}$ in solution. Positioning of the more bulky methoxypyridine subunits in the least sterically congested area of the complex is generally found in $[(\mathbf{L^{0\to2}})_2Cu]^+$. The dramatic diminution of intra- and inter-ligand exchange observed for $[(\mathbf{L^1})_2Cu]^+$ compared to $[(\mathbf{L^0})_2Cu]^+$ and $[(\mathbf{L^2})_2Cu]^+$ is thought to result from the energetically unfavorable substitution of a ligated 6-H-pyridine by an unligated methoxypyridine. As only this type of substitution is possible in $[(\mathbf{L^1})_2Cu]^+$, intra- and consequently inter-ligand exchange is slowed.

The series of “bis-tris” Cu(II) complexes, $[(\mathbf{L^{0\to3}})_2Cu]^{2+}$, shows a systematic tetragonal distortion as the steric requirements of the ligands are reduced; the 6-H-pyridines are preferentially positioned in the equatorial plane of the Cu(II). As observed for the Cu(I) complexes, $\mathbf{L^3}$ provides Cu(II) coordination arrangements different from the other three ligands. In $[(\mathbf{L^3})_2Cu]^{2+}$ one of the $\mathbf{L^3}$ is inverted to provide a *N*,*N'*,*O* facial-capping arrangement. Given the steric crowding within this complex, the decomposition to $[\mathbf{L^3}Cu(H_2O)_3]^{2+}$ in the presence of water is not surprising; however, the inverted coordination in $\mathbf{L^3}$ in this complex is curious. This simple series of methoxypyridine ligands indicates that interesting mononuclear metal coordination can result from appropriate substitution of all three pyridine subunits. The modular synthetic scheme allows for any type of substitution pattern at the periphery, such that protective cavities for a single metal may be created. The construction of such ligands and investigation of their chemistry are a current pursuit.

**Acknowledgment.** We are grateful to the National Institutes of Health (GM50730), the Petroleum Research Fund (28117-G3), and the Shell Career Initiation Award (T.D.P.S.) for financial support of this work. Mass spectra were performed by the Mass Spectrometry Facility, Department of Pharmaceutical Chemistry, University of California, San Francisco.

**Supporting Information Available:** ORTEP representations and complete tables of positional parameters, bond lengths, bond angles, and anisotropic thermal factors for all structures (129 pages). Ordering information is given on any current masthead page.

IC9713487

---

(49) Mahapatra, S.; Halfen, J. A.; Wilkinson, E. C.; Pan, G.; Wang, X. D.; Young, V. G., Jr.; Cramer, C. J.; Que, L., Jr.; Tolman, W. B. *J. Am. Chem. Soc.* **1996**, *118*, 11555−11574.

(50) Carrier, S. M.; Ruggiero, C. E.; Houser, R. P.; Tolman, W. B. *Inorg. Chem.* **1993**, *32*, 4889−4899.